Analysis of Helicopter Aeroelastic Characteristics in High-Speed Flight

WALTER GERSTENBERGER* AND EDWARD R. WOOD†
United Aircraft Coporation, Stratford, Conn.

Described is a general analytical method, which can be used for performance, stress, and vibration studies of helicopters and VTOL-type aircraft. The analysis is well suited for high-speed investigation, and applications are given for a helicopter in the flight regime from 80 to 160 knots. A sample problem is carried out at 150 knots. A rapidly convergent iterative procedure, which takes into account blade stall, is used to put the rotor in trim. Blade elemental lifts and drags are computed using wind tunnel airfoil data. Mach number effects are included. Blade motions are coupled to the aerodynamic excitation. Rotor blade dynamics are determined using a set of complex equations based upon an extension of Myklestad's analysis for rotating beams. The analysis assumes the blade infinitely rigid in torsion and takes into account 24 flatwise and 24 edgewise degrees-of-freedom with coupling due to built-in twist. There are provisions for handling rotor and propeller blades of all types: rigid, teetering, and articulated. Dynamics of the flexible blade are "married" to dynamics of the fuselage by matching blade root impedance to fuselage impedance at the rotor head. The resulting calculation gives the coupled blade-fuselage dynamic response at a particular airspeed.

Nomenclature

α_T = rotor angle of attack, positive for forward tilt of the tip-path plane
D_R = rotor drag
D_F = fuselage parasite drag
W_F = gross weight of helicopter
T = total rotor thrust
v_i = induced inflow velocity at rotor blade
λ_T = inflow ratio
Ω = rotor angular velocity
V = true airspeed of helicopter along flight path
R = blade radius from axis of rotation
μ = tip-speed ratio ($V \cos\alpha_T/\Omega R$)
b = number of rotor blades
e = distance from flapping or drag hinge to axis of rotation
r = distance of blade element from the axis of rotation
$\bar{r}$ = distance from flapping hinge to location of blade element
$\bar{r}_T$ = distance from flapping hinge to location of resultant steady thrust vector
$\bar{R}$ = distance from flapping hinge to tip of rotor blade
β_0 = rotor coning angle as related to the rotor tip-path plane
ψ = blade azimuth angle, measured from downwind position in direction of rotation
$\theta_\psi{}^i$ = blade pitch angle at particular azimuth position after the ith iteration; representative blade radius is taken at $0.7R$
$\theta_0{}^i$ = steady component of blade pitch angle after the ith iteration
$\theta_{ns}{}^i$ = $\sin(n\psi)$ component of blade pitch angle after the ith iteration
$\theta_{nc}{}^i$ = $\cos(n\psi)$ component of blade pitch angle after the ith iteration
$M_\psi{}^i$ = total moment of thrusts about the flapping hinge at a particular azimuth position after the ith iteration
$M_0{}^i$ = steady component of blade thrust moment after the ith iteration
$M_{ns}{}^i$ = $\sin(n\psi)$ component of blade thrust moment after the ith iteration
$M_{nc}{}^i$ = $\cos(n\psi)$ component of blade thrust moment after the ith iteration
ρ = mass density of air
c_n = blade-section chord at the nth blade station
U_T = component of resultant velocity at blade element, which is perpendicular to blade-span axis and to axis of rotation
U_P = component of resultant velocity at blade element, which is perpendicular to blade-span axis and to U_T
V_s = velocity of sound
ϕ = inflow angle at blade element
β_T = twist at blade element, measured from $0.7R$ where $\beta_T = 0$
α_b = blade element angle-of-attack
C_L = section two-dimensional lift coefficient
C_D = section two-dimensional drag coefficient
$F_n + jf_n$ = aerodynamic lift force acting on the nth blade element for a particular frequency component, $F_n \sin\omega t + f_n \cos\omega t$
$D_n + jd_n$ = aerodynamic drag force acting on the nth blade element for a particular frequency component, $D_n \sin\omega t + d_n \cos\omega t$
T_n = centrifugal tension force acting on the nth blade element, measured in a plane perpendicular to the axis of rotation
$S_n{}^F$ = flatwise shear force acting on the nth blade element, measured parallel to the axis of rotation
$S_n{}^E$ = edgewise shear force acting on the nth blade element, measured perpendicular to the blade-span axis and to axis of rotation
m_n = mass of nth blade element
ω = frequency
Z_n = flatwise displacement of nth blade station
X_n = edgewise displacement of nth blade station
C_n = flatwise aerodynamic damping constant for the nth blade station
$M_n{}^F$ = flatwise bending moment at nth blade station
$M_n{}^E$ = edgewise bending moment at nth blade station
$\theta_n{}^F$ = flatwise slope of the elastic axis at the nth blade station

Presented at the IAS 31st Annual Meeting, New York, January 21–23, 1963; revision received June 26, 1963. The method of analysis and data presented in this paper are the results of a three-year group effort in the Technical Branch at Sikorsky Aircraft. Credit for this work should be shared by the authors with K. D. Hilzinger and J. M. Moreno. K. D. Hilzinger was closely involved in setting up and checking the analysis. J. M. Moreno was responsible for computer programing and numerical analysis. Analytical development of the fuselage and coupling relationships was done by V. J. Rosa.

* Assistant Chief Engineer, Sikorsky Aircraft Division. Associate Fellow Member AIAA.
† Assistant Head, Dynamics Section, Sikorsky Aircraft Division. Member AIAA.

$\theta_n{}^E$ = edgewise slope of the elastic axis at the nth blade station

v,u,g,V,U,G = blade slope and deflection relationships, including coupling due to twist; these are defined in Appendix B

$Z_T,\theta_T{}^F,$ $M_T{}^F,S_T{}^F$ = flatwise displacement, slope, moment, and shear at blade tip, respectively

$X_T,\theta_T{}^E,$ $M_T{}^E,S_T{}^E$ = edgewise displacement, slope, moment, and shear at blade tip, respectively

$Z_0 \ldots S_0{}^E$ = same as above, corresponding flatwise and edgewise values for blade root

η_{0n},ζ_{0n} = flatwise, edgewise blade root displacements at $n\Omega$ frequency

$S_{\eta 0n},S_{\zeta 0n}$ = flatwise, edgewise blade root shears at $n\Omega$ frequency

X,Y,Z = displacements at the center of the rotor head in the fixed coordinate system

θ_F,ϕ_F,ψ_F = rotations at the center of the rotor head in the fixed coordinate system

S_x,S_y,S_{zz} M_{xx},M_{yy},M_{zz} = corresponding fixed system forces and moments

$[B_0]$ = blade amplitude and moment coefficients at root

$\{\eta_0\}$ = blade amplitude and moment response at root

$\{Z_F\}$ = total fuselage response at hub

$[R]$ = unit fuselage hub responses

$[\gamma]$ = coordinate transformation, fixed to rotating system

$\{S_F\}$ = forces and moments at hub in fixed system

$[\lambda]$ = force transformation, rotating to fixed system

$\{S_0\}$ = blade shears at root

$\{\eta_T\}$ = blade tip amplitudes and slopes

$[C_0]$ = blade shear coefficients at root

$\{\alpha_{\eta_0}\}$ = force constants, blade amplitude, and moment equations

$\{\alpha_{s0}\}$ = force constants, blade shear equations

$\{\alpha\}$ = coupled force equations

$[A]$ = coupled blade equations

Introduction

THE modern helicopter has reached the present state-of-the-art without waiting for a complete definition of its aerodynamic and dynamic characteristics. Instead, it has been designed by extrapolation of existing parameters, then allowed to prove itself by thorough flight test and development programs.

Of the three major areas of the aeroelastic problem (aerodynamics, blade dynamics, and fuselage dynamics), studies were made of each singly, or, at best, a combination of two at a time. Problems in each area are sufficiently complex to warrant further studies. Such studies may determine whether a simpler or more detailed approach can be used for a desired accuracy, but this is difficult to predict. A good example is the problem of defining the rotor's induced flow field during low-speed flight. Here, a more accurate determination is sorely needed to help define one of the roughest regimes of the helicopter as well as to shed light on the causes of peculiar control stick gradients and handling qualities.

Using high-speed digital computers, the scientist today can probe into areas previously inaccessible through the use of slide rules and hand computation. With modern computers it is possible to consider all three previously mentioned areas of the helicopter aeroelastic problem simultaneously. The following discussion will describe a method of determining the forced response of a rotor-fuselage system under the influence of aerodynamic exciting forces in high-speed flight.

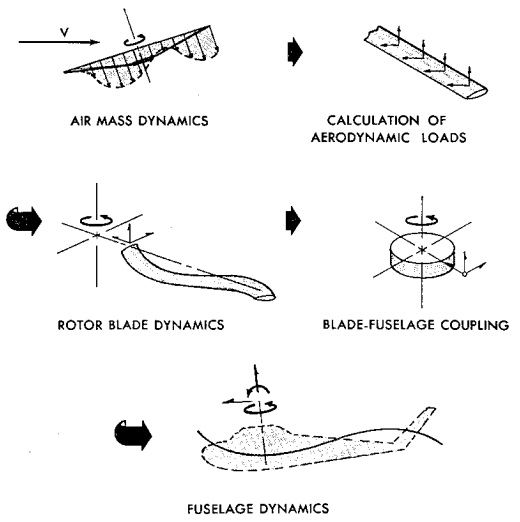

Fig. 1 Statement of the problem.

Approach to the Problem

The general helicopter aeroelastic problem can be subdivided into five major categories, as shown by Fig. 1. These are 1) air mass dynamics, 2) calculation of aerodynamic loads, 3) rotor blade dynamics, 4) blade-fuselage coupling, and 5) fuselage dynamics. The description of analysis, which follows, treats these topics in this order. The method is general and may be used to explore effects of flight, rotor, blade, and fuselage parameters on resulting blade motions, blade stresses, fuselage vibrations, and performance of an articulated, teetering, or rigid rotor system.

For an example, a conventional helicopter with fully articulated rotor head is considered. The gross weight, drag, speed, rotor angular velocity, quasi-steady state airfoil characteristics, structural stiffnesses, and mass distributions must be defined.

The rotor disk is considered to be moving at the proper forward tilt to provide enough propulsive force to overcome the net drag of the aircraft. It must also support the aircraft, and there must be sufficient cyclic pitch to keep the rotor in equilibrium. Certain simplifying assumptions are made to initiate the calculation, such as the approximate coning angle, an estimate of the rotor drag, and an estimate of the radial position of the resultant thrust vector. These approximations do not affect the final accuracy, for if they are too far in error, this can be remedied by a second or third iteration.

For a high-speed condition, constant inflow is taken. The blade is subdivided into 24 elements. For each of 36 10°-azimuth intervals, the blade is considered set at two blade angles. These angles bracket the expected blade angles. Blade-element aerodynamic lifts are then computed, from which the moment of the thrust about the flapping hinge is calculated as a function of blade angle and azimuth position. Stall and reverse flow effects are taken into account by using two-dimensional airfoil data for angles-of-attack to 360°. The cyclic pitch necessary to maintain the rotor system in equilibrium is then calculated by an iteration to enforce the condition that the first-harmonic thrust moment about the flapping hinge is zero.

Final determination of cyclic pitch yields angle-of-attack distribution, rotor drag, power required, location of resultant thrust vector, thrust moments, and resolved thrusts and drags on 24 blade elements for 10°-azimuth intervals. A harmonic analysis is performed on this loading, and the steady plus the first 11 harmonics of blade loading (thrust and drag) are obtained in complex form.

Harmonics of the airload calculation now are introduced into the blade dynamic analysis. These harmonics give rise to vibratory responses of the blade. Since the blade is restrained at the root, the blade responses result in root

shears, which feed from the rotor head into the fuselage as vibratory shears and moments. As the forces go from the rotating to the fixed fuselage system, the rotor system tends to act as a filter. For an n-bladed rotor system, the primary frequency that filters through is that at n/rev. It can be shown that n/rev fuselage vibrations in the fixed system are the result of $n - 1$, n, and $n + 1$/rev vibratory response of the blades in the rotating system.

Analysis for flexible blade dynamics is based upon an extension of Myklestad's analysis for rotating beams.[9] There is provision for up to 24 flatwise and 24 edgewise degrees-of-freedom with coupling due to twist. Equations are in complex form to allow for aerodynamic damping and phasing of aerodynamic loads. Boundary conditions at the tip of the blade require that shear and moment are zero. One of the boundary conditions at the root of the blade is that the moment about the flapping hinge is zero. The moment about the drag hinge is made equal to the damper coefficient times the angular velocity of the blade about the drag hinge. The other boundary conditions involve relationships between forces in three directions and their respective displacements, and moments about three perpendicular axes and their rotations. Dynamics of the flexible blade are coupled to dynamics of the fuselage by matching blade impedance to fuselage impedance at the rotor head. Fuselage impedance is obtained by a forced response analysis at the nth harmonic frequency. Since three frequencies are considered on the blade ($n - 1$, n, $n + 1$), and there are two blade equations flatwise and two equations edgewise for each frequency, a system of 12 complex simultaneous equations must be solved. Blade-fuselage coupling is shown schematically in Fig. 2.

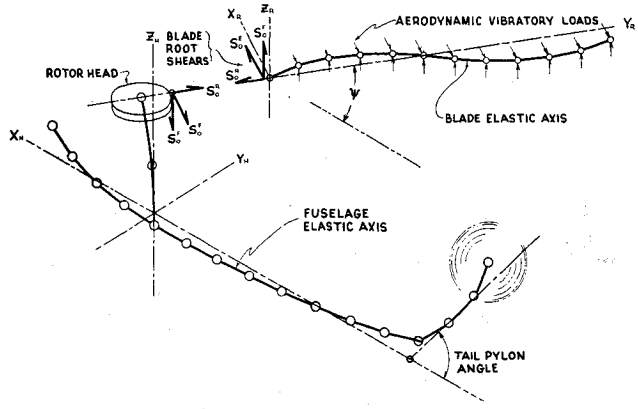

Fig. 2 Coupled blade-fuselage dynamic analysis.

Rotor Blade Dynamic Analysis

1) Based on extension of Myklestad's analysis for rotating beams.
2) Provides 24 flatwise and 24 edgewise blade degrees-of-freedom with coupling due to twist. Can include torsion.
3) Has provision for variable boundary conditions—easily amended for handling teetering or cantilevered blades.
4) Can be used for calculating vibratory response at a particular frequency, total blade response, or blade natural frequencies.
5) Simulates blade elastic curve, in contrast to methods which divide blade into rigid segments.
6) Has provision for a lag damper.
7) Aerodynamic damping included in the equations.
8) Allows for motion of rotor head.
9) Can be used for finding the response of blade to arbitrary excitations, such as stepped inputs.
10) Forced response analysis will yield flatwise and edgewise deflections, slopes, moments, shears, and stresses at each of the 24 blade stations for 10°-azimuth intervals.
11) Equations are in complex form. This yields phasing when calculating vibratory forced response of the blade at a particular frequency.

Blade-Fuselage Coupling

1) Dynamics of the flexible blade are "married" to dynamics of the fuselage by matching blade root impedance to fuselage impedance at the rotor head.
2) The "heart" of this analysis consists of two coordinate transformations, one relating forces in the rotating system to forces in the fixed system, the other relating angular and linear displacements in the rotating system to the fixed system.
3) Results of the calculation give the n/rev vertical and coupled-lateral-torsion fuselage response at a particular airspeed.
4) Also, obtained is the n-1, n, and $n + 1$/rev flatwise-edgewise blade response for that airspeed.

Fuselage Forced Response Analysis

1) Based on a direct inverse solution of the dynamic matrix.
2) Will handle up to 70 degrees-of-freedom.
3) Has provision for calculating the forced response due to any vibratory force or moment at any fuselage station or any combination of forces or moments.
4) Structural damping may be included.

For helicopter inflight blade studies, a total forced response analysis of the blades is used. This analysis, by superposition of 11 harmonics of vibratory response, yields flatwise and edgewise deflections, moments, shears, and stresses at each of 24 blade stations for 10°-azimuth intervals.

Calculations presented in this paper were done on an IBM 7090 computer. Figure 3 shows a flow chart that links the various sections of the analysis. This chart illustrates the machine procedure for combining each part of the problem. Results of inflow calculations and two-dimensional wind tunnel data are seen linked to rotor trim and airload calculations. Airloads provide the excitation for the rotor blade. Blade response, in turn, depends upon boundary conditions that are dictated by hub impedance relations. The resulting calculation gives the fuselage vibratory response, and both individual harmonics and total response of the blade.

Definition of Parameters

Before developing the method of aeroelastic analysis, first define the basic parameters.‡ These specify the geometry of the vehicle system and provide the framework upon which the analysis is constructed. The parameters will be defined for a specific example. This will serve to give more meaning to the development of equations that follow.

Consider a five-bladed helicopter, flying in unaccelerated level flight at a speed of 150 knots. Gross weight of the aircraft is 13,600 lb. Parasite drag on the fuselage is 870 lb, based upon an equivalent flat plate area of 11.4 ft^2. Rotor radius is 28 ft and rotational speed is 222 rpm. This results in a tip speed of 650 fps and an advance ratio of approximately 0.388.

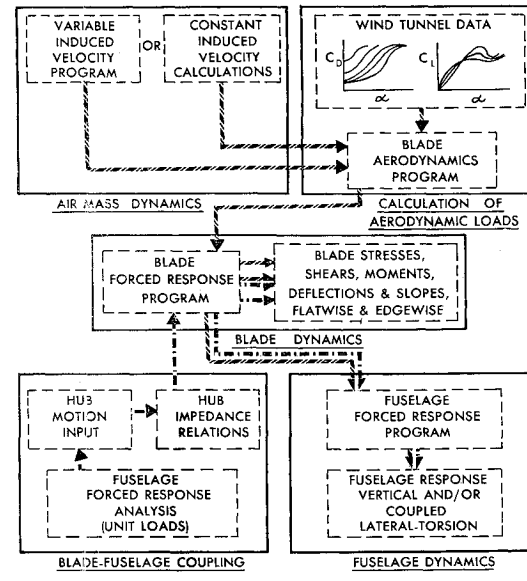

Fig. 3 Block diagram for aeroelastic analysis.

‡ The high-speed helicopter described herein will be referred to as hsh. Parameters given are similar to those of the Sikorsky high performance helicopter (hph). This helicopter was the subject of a design study for the U. S. Army Transportation Research Command and an American Helicopter Society paper.[14,15]

The helicopter considered has a fully articulated rotor system. Flapping and lag hinges are coincident and located 12.625 in. from the center of rotation. Rotor disk solidity is 0.086, which results in a blade chord of 18.25 in. for a uniform or nontapered blade. There is a lag damper with a damping coefficient of 32,506 lb-in.-sec.

Rotor blades are of aluminum spar-type construction with bonded metal pockets. With the exception of the root region, the blades are essentially uniform in structural and weight properties. At the 50% radius point, values for flatwise and edgewise blade moments of inertia are 2.5 and 27 in.^{4}, respectively. Weight per unit length at this point is 0.5 lb/in. Airfoil cross section is an NACA 0012. The blade is twisted $-4°$. Also, for this blade, the elastic axis, center of gravity, and aerodynamic center are coincident along the spar, located at the quarter chord.

For calculation of aerodynamic loads, two-dimensional airfoil data are used. Compressibility effects are taken into account by using C_L vs α and C_D vs α curves for angles-of-attack from 0 to 30°, defining a family of C_L, C_D curves in 5% increments for Mach numbers up to 0.95. To define stall regions above angles-of-attack of 30°, a single C_L vs α and C_D vs α curve was taken from Ref. 13.

Dynamic response characteristics of the fuselage are given in Table 1. Presented are responses at the rotor head to 5/rev unit shears and moments in the fixed coordinate system. These were obtained by the method given in Appendix C. Fuselage panel-point mass and stiffness properties are required to calculate the dynamic response of the airframe. In the analysis to be described, blades are coupled to vertical and coupled-lateral-torsion fuselage responses. The zeros, which appear in Table 1, are due to decoupling of the vertical from the lateral-torsion responses. Also, since the numbers presented are real, no fuselage damping has been included in the sample problem.

Table 1 Fuselage rotor head response at 5/*rev* (1110 cpm)

UNIT APPLIED LOAD OR MOMENT		DISPLACEMENT OR ROTATION TO APPLIED LOAD OR MOMENT [a]					
		X	Y	Z	Φ_F	Θ_F	Ψ_F
	Sx	1093.85	0	-217.247	0	67.4804	0
	Sy	0	-532.073	0	20.0203	0	-.87227
	Sz	-217.247	0	-103.287	0	-6.59514	0
	Mxx	0	20.0203	0	3.79265	0	-.013704
	Myy	67.4804	0	-6.59514	0	5.17107	.0
	Mzz	0	-.87227	0	-.013704	0	-.012696

Part I: Description of Analysis

Aerodynamic Solution

Induced Velocity

The aerodynamic analysis is initiated by solving for the induced velocity through the rotor disk. For speeds above 100 knots, inflow is assumed constant over the rotor disk and induced velocity calculated by Wheatley's equation.[6]

Taking a tip-path plane coordinate system as a reference for zero flapping (Fig. 4), calculations are started by assuming rotor thrust normal to the tip-path plane. An estimate is made for the presence of a force in the plane of rotation. Corrections may be made by a second iteration. Solving for rotor angle-of-attack,

$$\alpha_T = \tan^{-1}\frac{D_F + D_R}{W_F - L_F} = \frac{870 + 220}{13{,}600} = 4.585° \qquad (1)$$

where

D_F = fuselage parasite drag, lb
D_R = estimated rotor drag, lb
W_F = gross weight of aircraft, lb
L_F = lift on fuselage plus attached aerodynamic surfaces, lb

and rotor thrust T becomes

$$T = \frac{W_F - L_F}{\cos\alpha_T} = \frac{13{,}600}{0.9968} = 13{,}644\,\text{lb} \qquad (2)$$

The induced velocity may now be determined as follows. From Ref. 6,

$$\lambda_T = \mu\sin\alpha_T + \frac{\frac{1}{2}C_T}{(\lambda_T^2 + \mu^2)^{1/2}} \qquad (3)$$

This equation can be solved rapidly by iterating, taking λ_T as zero for the first iteration. For this sample problem, there results $\lambda_T = 0.0382$. From this the induced velocity is readily obtained, since by definition

$$v_i = \lambda_T\Omega R - V\sin\alpha_T = 4.58\ \text{fps} \qquad (4)$$

Thrust Moment-Blade Angle Iteration

An interesting feature of this analysis, which will be described in detail, is the method by which cyclic pitch is computed. This is an iterative process in which there is set up a plot of blade angle vs thrust moment for each azimuth position. Blade cyclic is determined by repeatedly removing all but the first harmonic from the cyclic pitch, and at the same time insuring that there is no first-harmonic flapping by forcing the first harmonic of the thrust moment to go to zero. The condition for zero first-harmonic thrust moment satisfies the boundary condition of no steady pitching or rolling moment applied to the rotor head in fixed coordinates.

The computer method now used for placing the rotor in trim is based on a graphical method developed earlier for balancing cyclic pitch and thrust moments. This method, given in Appendix A, is particularly useful in providing a physical picture of requirements to be met by a rotor in high-speed flight.

Continuing to initialize the calculation, approximate the coning angle by assuming the thrust to act at 0.70 radius. This is shown in Fig. 5. The approximate coning angle determined by summing moments is

$$\sin\beta_0 = \frac{\dfrac{T}{b}\bar{r}_T - \displaystyle\sum_0^{\bar{R}}\bar{r}dw}{\displaystyle\sum_0^{\bar{R}}\bar{r}(e + \bar{r})\Omega^2 dm} \qquad (5)$$

where b = number of blades, $\bar{r} = (r - e)$, and $\bar{R} = (R - e)$.

The numerator of this expression is the mean thrust moment required, M_0. The problem is to find the steady and cyclic blade angles necessary to produce the desired thrusts and thrust moments to keep the rotor in trim.

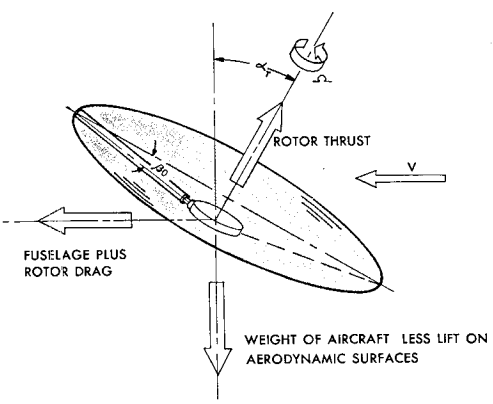

Fig. 4 Tip-path plane system.

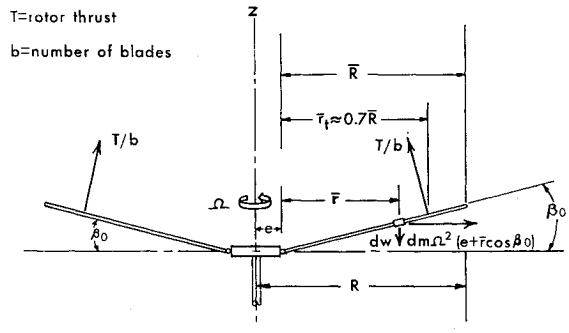

Fig. 5 Diagram for approximate coning angle.

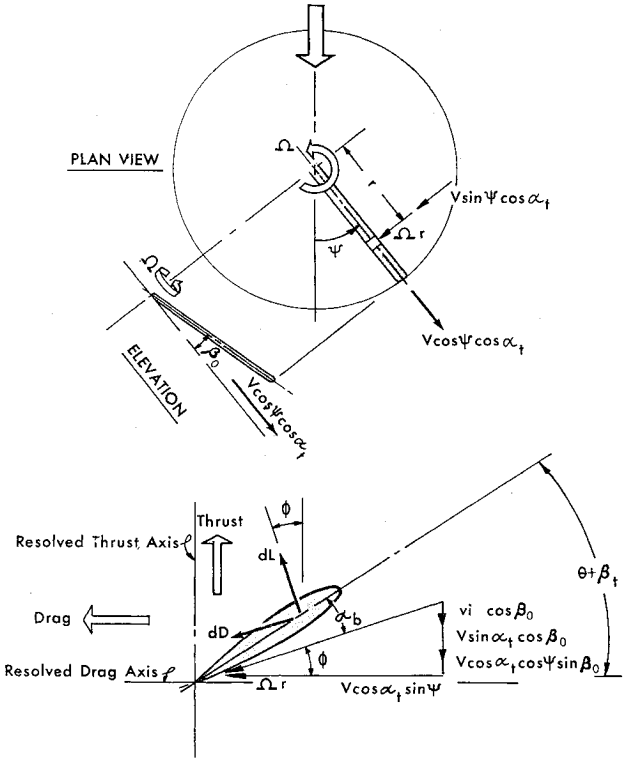

Fig. 6 Blade element aerodynamics.

Assume values of blade angles, which can be generated by cyclic pitch control of the helicopter. In other words, assume a steady component and a first-harmonic cyclic pitch such as given below:

$$\theta_\psi{}^1 = \theta_0{}^1 + \theta_{1s}{}^1 \sin\psi + \theta_{1c}{}^1 \cos\psi$$

Refer to Fig. 6. With blade angles defined for each azimuth position, one can now calculate corresponding thrust moments from the relation

$$M_\psi(\psi,\theta) = \sum_{r=e}^{r=R} \frac{\rho}{2} c_n r dr [U_P{}^2 + U_T{}^2]_n [C_L \cos\phi - C_D \sin\phi]_n \tag{6}$$

where the subscript n denotes the nth blade element. In this expression,

$$U_P = v_i \cos\beta_0 + V \sin\alpha_T \cos\beta_0 + V \cos\alpha_T \cos\psi \sin\beta_0 \tag{7}$$

$$U_T = \Omega r + V \cos\alpha_T \sin\psi \tag{8}$$

and blade element angle-of-attack is

$$\alpha_b = \theta_\psi + \beta_T - \phi \tag{9}$$

where ϕ is the inflow angle, determined from

$$\phi = \tan^{-1}(U_P/U_T) \tag{10}$$

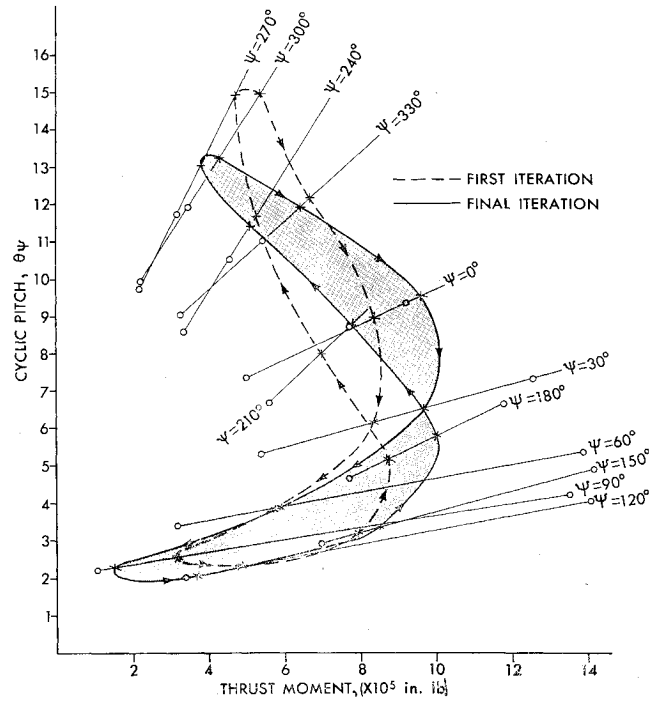

Fig. 7 Cyclic pitch-thrust moment iteration.

with differential lifts and drags for the nth blade element:

$$dL = (\rho/2) C_{Lc_n} dr [U_P{}^2 + U_T{}^2]_n \tag{11}$$

$$dD = (\rho/2) C_{Dc_n} dr [U_P{}^2 + U_T{}^2]_n \tag{12}$$

For the coefficients of lift and drag, two-dimensional airfoil data are used, Mach number being determined by

$$\text{Mach no.} = (U_P{}^2 + U_T{}^2)^{1/2}/V_s \tag{13}$$

Thirty-six azimuth positions are taken to obtain accuracy for the higher harmonics. These thrust moments will contain first-harmonic components. It is necessary to remove the first-harmonic components and refine the steady component. This is done with the following equation:

$$\Delta M = M_\psi{}^2 - M_\psi{}^1 = -M_0{}^1 + M_0{}^0 - M_{1s}{}^1 \sin\psi - M_{1c}{}^1 \cos\psi \tag{14}$$

where

$$M_0{}^1 = \frac{\sum_{\psi=0°}^{\psi=350°} M_\psi{}^1}{36} \tag{15}$$

and

$$M_{1s}{}^1 = \frac{\sum_{\psi=0°}^{\psi=350°} M_\psi{}^1 \sin\psi}{18} \tag{16}$$

$$M_{1c}{}^1 = \frac{\sum_{\psi=0°}^{\psi=350°} M_\psi{}^1 \cos\psi}{18} \tag{17}$$

At this point it is necessary to calculate thrust moments for another set of blade angles, slightly larger than the original set. To determine change in thrust moment with small change in blade angle, a second approximation to blade angle is given by the following:

$$\theta_\psi{}^2 = \theta_\psi{}^1 + (\partial\theta_\psi/\partial M_\psi)\Delta M \tag{18}$$

Blade angles at each azimuth position are next refined by analyzing for the steady and first-harmonic components. These values become the new cyclic pitch, since this is the

type of control enforced by the helicopter swashplate. In other words,

$$\theta_\psi{}^3 = \theta_0{}^2 + \theta_{1s}{}^2 \sin\psi + \theta_{1c}{}^2 \cos\psi \qquad (19)$$

This iteration continues until the higher-harmonic content of cyclic pitch and first-harmonic content of thrust moment converge on zero. Figure 7 shows the results after the first and last iterations. Illustrated is the 150-knot flight condition of the sample problem. The resulting two-loop Lissajou figure approximates that of pure first- and second-harmonic functions with a phase angle of about 25°. The 90 and 270° points would be vertically in line with each other, if the thrust moment contained only second harmonic. The amount of dissymmetry indicates the degree of third- and higher-harmonic content present in the thrust moment.

The iteration has been found to converge rapidly at airspeeds where the blade is relatively unstalled. As the blade becomes progressively stalled, the number of iterations increases. Referring to Fig. 7, as airspeed increases, the 90 and 270° points move to the left. This means the 90 and 270° thrust moments become progressively smaller for higher airspeeds. Greater demand is placed on the rotor at other azimuth positions to satisfy the mean thrust moment required.

With blade angles defined, final blade element lift and drag forces are determined once more using two-dimensional airfoil data. Forces are resolved into a steady and 11 harmonic components. These may be expressed in complex form as given below:

$$F_\psi = F_0 + \sum_{n=1}^{n=11} \Re(f_{nc} - jF_{ns})e^{jn\psi} \qquad (20)$$

All harmonics of these forces contribute to response of the blade. But as forces go from the rotating to the fixed fuselage system, the rotor system tends to act as a filter, and the only harmonics that will combine when the five blades are summed are the fourth, fifth, and sixth; ninth, tenth, and eleventh; etc. Since the lower harmonics of blade loading are considerably greater than the higher, experience has shown that 5/rev vibration of the fuselage is most critical. For this reason one need only consider the fourth-, fifth-, and sixth-harmonics of this five-bladed rotor system.

Rotor Blade Dynamics

Rotor blade dynamics are determined using a set of equations in complex form based upon an extension of Myklestad's analysis for rotating beams.[9] The coupled flatwise-chordwise equations are designed to receive the individual harmonics of lift and drag computed as just described. These harmonics, which are of the form $a_n \sin(n\psi) + b_n \cos(n\psi)$ result in separate complex vibratory blade responses, which are finally superimposed to yield the total response of the blade at 36 azimuth intervals. A tip-path plane coordinate system is used.

Figures 8a,b illustrate an element of the blade with the dynamic forces and moments acting on it. Both flatwise and edgewise projections are given.

Summing forces on this element, the centrifugal tension will be given by

$$T_n = T_{n+1} + m_n\Omega^2 r_n \qquad (21)$$

Flatwise and edgewise shears may be written as

$$S_n{}^F = S^F{}_{n+1} + m_n\omega^2 Z_n - jC_n\omega Z_n + F_n + jf_n \qquad (22)$$

$$S_n{}^E = S^E{}_{n+1} + m_n(\omega^2 + \Omega^2)X_n + D_n + jd_n \qquad (23)$$

The term C_n represents the flatwise aerodynamic damping on the blade element, and can be expressed by

$$C_n = 5.73(\text{chord})_n(l_{n,n+1})(\rho/2)(\Omega r_n) \qquad (24)$$

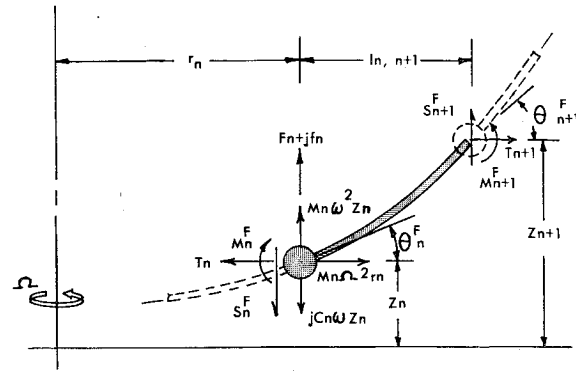

Fig. 8a Blade element equilibrium; flatwise system.

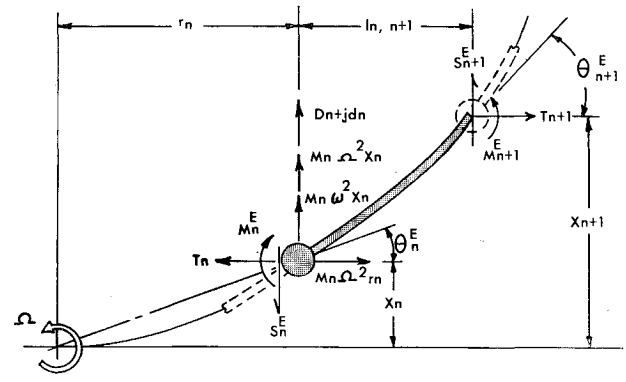

Fig. 8b Blade element equilibrium; edgewise system.

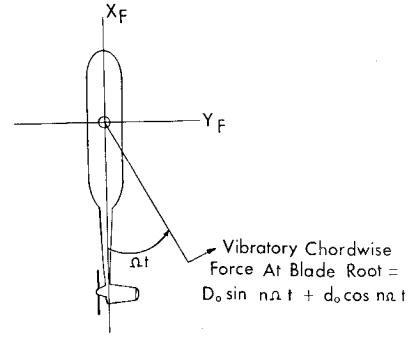

Fig. 8c Chordwise force rotating to fixed coordinates.

Real and imaginary flatwise and edgewise equations for moment, slope, and deflection are the same. Writing the real equations, one obtains

$$M_n{}^F = M^F{}_{n+1} + S^F{}_{n+1}l_{n,n+1} - T_{n+1}(Z_{n+1} - Z_n) \qquad (25)$$

$$\theta_n{}^F = \theta^F{}_{n+1}(1 + T_{n+1}u_{zz}) + T_{n+1}\theta^E{}_{n+1}u_{zx} - M^F{}_{n+1}v_{zz} - M^E{}_{n+1}v_{zx} - S^F{}_{n+1}u_{zz} - S^E{}_{n+1}u_{zx} \qquad (26)$$

$$Z_n = Z_{n+1} - \theta_n{}^F l_{n,n+1} + T_{n+1}\theta^F{}_{n+1}g_{zz} + T_{n+1}\theta^E{}_{n+1}g_{zx} - M^F{}_{n+1}u_{zz} - M^E{}_{n+1}u_{zx} - S^F{}_{n+1}g_{zz} - S^E{}_{n+1}g_{zx} \qquad (27)$$

$$M_n{}^E = M^E{}_{n+1} + S^E{}_{n+1}l_{n,n+1} - T_{n+1}(X_{n+1} - X_n) \qquad (28)$$

$$\theta_n{}^E = \theta^E{}_{n+1}(1 + T_{n+1}U_{xx}) + T_{n+1}\theta^F{}_{n+1}U_{xz} - M^E{}_{n+1}V_{xx} - M^F{}_{n+1}V_{xz} - S^E{}_{n+1}U_{xx} - S^F{}_{n+1}U_{xz} \qquad (29)$$

$$X_n{}^E = X^E{}_{n+1} - \theta_n{}^E l_{n,n+1} + T_{n+1}\theta^E{}_{n+1}G_{xx} + T_{n+1}\theta^F{}_{n+1}G_{xz} - M^E{}_{n+1}U_{xx} - M^F{}_{n+1}U_{xz} - S^E{}_{n+1}G_{xx} - S^F{}_{n+1}G_{xz} \qquad (30)$$

It will be noted that the coordinate system chosen is such that flatwise and edgewise force and moment equations are uncoupled. Coupling terms due to twist appear entirely in the slope and deflection equations.

Before applying these equations to a specific blade-fuselage system, consider their general form prior to substituting

boundary conditions for either end of the blade. Integrating blade elements from tip to root, the shears, moments, slopes, and deflections at the blade root may be expressed in terms of corresponding unknown tip values. For each harmonic an 8×8 matrix as shown below would result:

$$\begin{bmatrix} S_0{}^F \\ M_0{}^F \\ \theta_0{}^F \\ Z_0 \\ S_0{}^E \\ M_0{}^E \\ \theta_0{}^E \\ X_0 \end{bmatrix} = \begin{bmatrix} d_{11} & d_{12} & d_{13} & d_{14} & d_{15} & d_{16} & d_{17} & d_{18} \\ d_{21} & d_{22} & d_{23} & d_{24} & . & . & . & . \\ d_{31} & d_{32} & . & . & . & . & . & . \\ . & . & . & . & . & . & . & . \\ . & . & . & . & . & . & . & . \\ . & . & . & . & . & . & . & . \\ . & . & . & . & . & . & . & . \\ . & . & . & . & . & . & . & . \end{bmatrix} \begin{bmatrix} S_T{}^F \\ M_T{}^F \\ \theta_T{}^F \\ Z_T \\ S_T{}^E \\ M_T{}^E \\ \theta_T{}^E \\ X_T \end{bmatrix} + \begin{bmatrix} \alpha_{s0}{}^F \\ \alpha_{M0}{}^F \\ \alpha_{\theta 0}{}^F \\ \alpha_{z0}{}^F \\ \alpha_{s0}{}^E \\ \alpha_{M0}{}^E \\ \alpha_{\theta 0}{}^E \\ \alpha_{z0}{}^E \end{bmatrix} \tag{31a}$$

or

$$\{\zeta_0\} = [D_0]\{\zeta_T\} + \{\alpha_{\zeta 0}\} \tag{31b}$$

In Eq. (31), the subscript 0 denotes the root variable and the subscript T the tip variable. Column matrices of shears, moments, slopes, and deflections are complex, as is the force or $\{\alpha_{\zeta 0}\}$ column matrix. Constants in the 8×8 blade matrix, $[D_0]$, are also complex. These values result from the integration and reflect frequency as well as blade mass and stiffness properties.

In the case of coupled flatwise and edgewise vibrations, four boundary conditions must be satisfied at each end of the blade. Application of tip boundary conditions eliminates four unknowns in Eq. (31). The resulting blade matrix $[D_0]$ to be solved is a 4×4.

For conventional free-ended helicopter blades, tip shears and tip moments are zero. Solution of the blade's forced dynamic response is obtained by 1) applying appropriate root boundary conditions, 2) inverting the 4×4 complex blade matrix, and 3) solving for unknown flatwise and edgewise tip slopes and deflections.

Root boundary conditions are determined by 1) the root construction of the blade (articulated, teetering, or rigid) and 2) blade-fuselage coupling relationships. Rotor blades are coupled to the fuselage by matching blade root impedance to fuselage impedance through two transformations. One relates moments and forces in the rotating system to moments and forces in the fixed system. The other relates angular and linear displacements in the rotating system to the fixed system. Moments, forces, and coordinates to be related depend upon the root construction of the blade.

To understand how blades are coupled to the fuselage, first explore root conditions for the case of infinite rotor head impedance. Here, blades are decoupled from the fuselage and the root conditions depend only on blade root restraint. Boundary conditions are given below for the articulated rotor system considered here, i.e., the articulated blade with lag damper:

$$M_0{}^F = 0 \qquad Z_0 = 0$$
$$M_0{}^E - jC_\theta \omega \theta_0{}^E = 0 \qquad X_0 = 0 \tag{32}$$

for all harmonics.

Blade-Fuselage Coupling

Consider the case where the fuselage impedance is not infinite. Here, fuselage impedance must be matched to the blade root boundary condition. The problem is complicated by the transfer from rotating to fixed coordinates. This transfer determines which blade harmonics must be considered. Begin by looking at the relationship between a vibratory force in a rotating system and the resultant excitation in a fixed coordinate system. Take a simple example as shown in Fig. 8c:

$$F_x = D_0 \sin n\Omega t \sin \Omega t + d_0 \cos n\Omega t \sin \Omega t$$
$$F_x = (D_0/2)\sin(n+1)\Omega t - (d_0/2)\sin(n-1)\Omega t \tag{33}$$

Equation (33) shows that a fore and aft force at frequencies of $(n+1)\Omega$ and $(n-1)\Omega$ results in the fixed coordinate system from a vibratory inplane force at a frequency of $n\Omega$ in the rotating system. In other words, there is a $\pm 1\Omega$ frequency shift for inplane forces going from rotating to fixed coordinates. Pitching and rolling moments are similar rotating vectors and follow the same relationship. For vectors normal to the plane of rotation, along the Z axis, it can be seen that there will be no frequency change. Vertical forces at the root of the blade and yawing moments are examples of these vectors.

It can be shown for an n-bladed rotor system that, assuming all blades see the same loading at the same azimuth position, only the $n\Omega$ frequency will be seen in the fixed system. As just has been seen, this $n\Omega$ frequency in the fixed system can arise from either $n-1$, n, or $n+1$ excitation in the rotating system. To see why only $n\Omega$ is filtered through, take b blades and let $n\Omega$ be the frequency:

Vertical Force

$$F_z = F\sin(n\Omega t) + F\sin n\left(\Omega t + \frac{2\pi}{b}\right) + F\sin n\left(\Omega t + \frac{4\pi}{b}\right) + \ldots \tag{34a}$$

or

$$F_z = \sum_{i=0}^{i=b} F\sin n\left(\Omega t + \frac{2\pi i}{b}\right) \tag{34b}$$

$F_z = bF$ when $n = b, 2b, 3b, \ldots$, etc., otherwise, $F_z = 0$. The following applies to the five-bladed articulated helicopter:

1) Flatwise 4 and 6/rev blade root shears will feed into the fuselage as 5/rev pitching and rolling moments.

2) Edgewise 4 and 6/rev shears produce fore and aft and lateral 5/rev forces at the rotor head.

3) Flatwise 5/rev shears feed directly through into the fuselage as a vertical 5/rev force.

4) Edgewise 5/rev blade shears apply a 5/rev yawing moment to the fuselage.

Figure 9 gives the coordinate system used for blade-fuselage coupling. The blade-fuselage coupling analysis is initiated by determining the 4, 5, and 6/rev coupled flatwise-edgewise blade dynamic response. Results of this blade analysis can be set up in matrix form as shown below. The resulting matrices are 12×12 and complex in form; subscripts refer to the harmonics:

$$\begin{bmatrix} Z_{04} \\ X_{04} \\ M_{04}{}^F \\ M_{04}{}^E \\ Z_{05} \\ X_{05} \\ M_{05}{}^F \\ M_{05}{}^E \\ Z_{06} \\ X_{06} \\ M_{06}{}^F \\ M_{06}{}^E \end{bmatrix} = \left[\begin{array}{c|c|c} B_{04} & 0 & 0 \\ \hline 0 & B_{05} & 0 \\ \hline 0 & 0 & B_{06} \end{array}\right] \begin{bmatrix} Z_{T4} \\ \theta_{T4}{}^F \\ X_{T4} \\ \theta_{T4}{}^E \\ Z_{T5} \\ \theta_{T5}{}^F \\ X_{T5} \\ \theta_{T5}{}^E \\ Z_{T6} \\ \theta_{T6}{}^F \\ X_{T6} \\ \theta_{T6}{}^E \end{bmatrix} + \begin{bmatrix} \alpha_{\eta 04} \\ \hline \alpha_{\eta 05} \\ \hline \alpha_{\eta 06} \end{bmatrix} \tag{35a}$$

or

$$\{\eta_0\} = [B_0]\{\eta_T\} + \{\alpha_{\eta_0}\} \tag{35b}$$

Blade Amplitude and Moment Equations

A similar matrix can be set up for the blade shear equations:

$$\begin{bmatrix} S_{04^F} \\ S_{04^E} \\ 0 \\ 0 \\ S_{05^F} \\ S_{05^E} \\ 0 \\ 0 \\ S_{06^F} \\ S_{06^E} \\ 0 \\ 0 \end{bmatrix} = \left[\begin{array}{c|c|c} C_{04} & 0 & 0 \\ \hline 0 & C_{05} & 0 \\ \hline 0 & 0 & C_{06} \end{array}\right] \begin{bmatrix} Z_{T4} \\ \theta_{T4^F} \\ X_{T4} \\ \theta_{T4^E} \\ Z_{T5} \\ \theta_{T5^F} \\ X_{T5} \\ \theta_{T5^E} \\ Z_{T6} \\ \theta_{T6^F} \\ X_{T6} \\ \theta_{T6^E} \end{bmatrix} + \begin{bmatrix} \\ \alpha_{s04} \\ \\ \hline \\ \alpha_{s05} \\ \\ \hline \\ \alpha_{s06} \\ \\ \end{bmatrix} \tag{36a}$$

or

$$\{S_0\} = [C_0]\{\eta_T\} + \{\alpha_{s0}\} \tag{36b}$$

Blade Shear Equations

The next step in coupling blades to the fuselage is to relate displacements in fixed fuselage coordinates to rotating blade root coordinates. Here, the assumption is made that the helicopter is in steady-state forward flight and each blade sees the same instantaneous load when at the same azimuth position. Converting displacements, one obtains

$$\begin{bmatrix} \eta_{04} \\ \zeta_{04} \\ \eta_{05} \\ \zeta_{05} \\ \eta_{06} \\ \zeta_{06} \end{bmatrix} = \begin{bmatrix} 0 & 0 & 0 & -j(e/2) & e/2 & 0 \\ j\frac{1}{2} & \frac{1}{2} & 0 & 0 & 0 & 0 \\ 0 & 0 & 1 & 0 & 0 & 0 \\ 0 & 0 & 0 & 0 & 0 & e \\ 0 & 0 & 0 & j(e/2) & e/2 & 0 \\ -j\frac{1}{2} & \frac{1}{2} & 0 & 0 & 0 & 0 \end{bmatrix} \begin{bmatrix} X \\ Y \\ Z \\ \theta_F \\ \phi_F \\ \psi_F \end{bmatrix} \tag{37a}$$

or

$$\{\eta_0\} = [\gamma]\{Z_F\} \tag{37b}$$

where $[\gamma]$ is the transformation relating displacements in the fixed X, Y, Z system to displacements in the moving ζ, η system. Here, X, Y, Z, θ_F . . . is of the form $a + bj = a\sin 5\psi + b\cos 5\psi$, etc., and, η_{04}, ζ_{04}, η_{05} . . . is of the form $c + dj = c\sin 4\psi + d\cos 4\psi$, etc.

Similarly, forces in the rotating blade coordinate system may be related to forces in the fixed fuselage system by means of the following transformation:

$$\begin{bmatrix} S_x \\ S_y \\ S_z \\ M_{xx} \\ M_{yy} \\ M_{zz} \end{bmatrix} = \begin{bmatrix} 0 & \frac{5}{2}j & 0 & 0 & 0 & -\frac{5}{2}j \\ 0 & \frac{5}{2} & 0 & 0 & 0 & \frac{5}{2} \\ 0 & 0 & 5 & 0 & 0 & 0 \\ \frac{5}{2}ej & 0 & 0 & 0 & -\frac{5}{2}ej & 0 \\ \frac{5}{2}e & 0 & 0 & 0 & \frac{5}{2}e & 0 \\ 0 & 0 & 0 & 5e & 0 & 0 \end{bmatrix} \begin{bmatrix} S_{\eta_{04}} \\ S_{\zeta_{04}} \\ S_{\eta_{05}} \\ S_{\zeta_{05}} \\ S_{\eta_{06}} \\ S_{\zeta_{06}} \end{bmatrix} \tag{38a}$$

or

$$\{S_F\} = [\lambda]\{S_{\eta_0}\} \tag{38b}$$

where $[\lambda]$ is the transformation relating forces in the rotating ζ, η system to forces in the fixed X, Y, Z system; where S_x, S_y . . . is of the form $a + bj = a\sin 5\psi + b\cos 5\psi$, etc.; and $S_{\eta_{04}}$, $S_{\zeta_{04}}$ . . . is of the form $c + dj = c\sin 4\psi + d\cos 4\psi$, etc.

Impedance of the rotor head is determined by treating the fuselage as a classical multi-degree-of-freedom system. A standard Lagrangean approach is used to obtain the vertical and coupled-lateral-torsion vibratory response. This will be discussed in more detail in the next section. Applying unit vibratory forces and moments to the rotor head at n/rev in fixed coordinates yields the response matrix $[R]$:

$$\begin{bmatrix} X \\ Y \\ Z \\ \theta_F \\ \phi_F \\ \psi_F \end{bmatrix} = \begin{bmatrix} R_{xx} & R_{xy} & R_{xz} & C_{xx} & C_{xy} & C_{xz} \\ R_{yx} & R_{yy} & R_{yz} & C_{yx} & C_{yy} & C_{yz} \\ R_{zx} & R_{zy} & R_{zz} & C_{zx} & C_{zy} & C_{zz} \\ \phi_{xx} & \phi_{xy} & \phi_{xz} & \Phi_{xx} & \Phi_{xy} & \Phi_{xz} \\ \phi_{yx} & \phi_{yy} & \phi_{yz} & \Phi_{yx} & \Phi_{yy} & \Phi_{yz} \\ \phi_{zx} & \phi_{zy} & \phi_{zz} & \Phi_{zx} & \Phi_{zy} & \Phi_{zz} \end{bmatrix} \begin{bmatrix} S_x \\ S_y \\ S_z \\ M_{xx} \\ M_{yy} \\ M_{zz} \end{bmatrix} \tag{39a}$$

or

$$\{Z_F\} = [R]\{S_F\} \tag{39b}$$

The rotor blades can now be "married" to the fuselage and the resultant $n - 1$, n, and $n + 1$/rev blade responses determined as follows.

Marriage of Blades to Fuselage

Blade Amplitude and Moment Equations

$$\{\eta_0\} = [B_0]\{\eta_T\} + \{\alpha_{\eta_0}\} \tag{35}$$

Blade Shear Equations

$$\{S_0\} = [C_0]\{\eta_T\} + \{\alpha_{s0}\} \tag{36}$$

Fuselage Response

$$\{Z_F\} = [R]\{S_F\} \tag{39}$$

Coupling Relationships

$$\{\eta_0\} = [\gamma]\{Z_F\} \tag{37}$$

$$\{S_F\} = [\lambda]\{S_{\eta_0}\} \tag{38}$$

therefore,

$$\{\eta_0\} = [\gamma][R][\lambda][C_0]\{\eta_T\} + [\gamma][R][\lambda]\{\alpha_{s0}\}$$

$$[B_0]\{\eta_T\} = [\gamma][R][\lambda][C_0]\{\eta_T\} + [\gamma][R][\lambda]\{\alpha_{s0}\} - \{\alpha_{\eta_0}\}$$

$$([B_0] - [\gamma][R][\lambda][C_0])\{\eta_T\} = [\gamma][R][\lambda]\{\alpha_{s0}\} - \{\alpha_{\eta_0}\} \tag{40}$$

or

$$[A]\{\eta_T\} = \{\alpha\} \tag{41a}$$

and

$$\{\eta_T\} = [A^{-1}]\{\alpha\} \tag{41b}$$

Once the unknown tip values, $\{\eta_T\}$, have been determined the resultant blade responses can be calculated by 1) either going through the blade equations once more with these values in place of the previously unknown Z_T, θ_{T^F}, X_T, and θ_{T^E} or 2) multiply the tip values by blade matrices, similar to the root matrix, which have been saved for each station during the blade integration.

Figures 10 and 11 show the fourth-, fifth-, and sixth-harmonic blade responses for the sample 150-knot helicopter. Note that blade root deflections have a finite value, indicating rotor head motion.

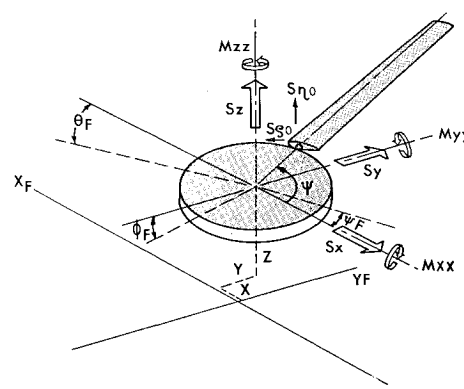

Fig. 9 Blade-fuselage coupling.

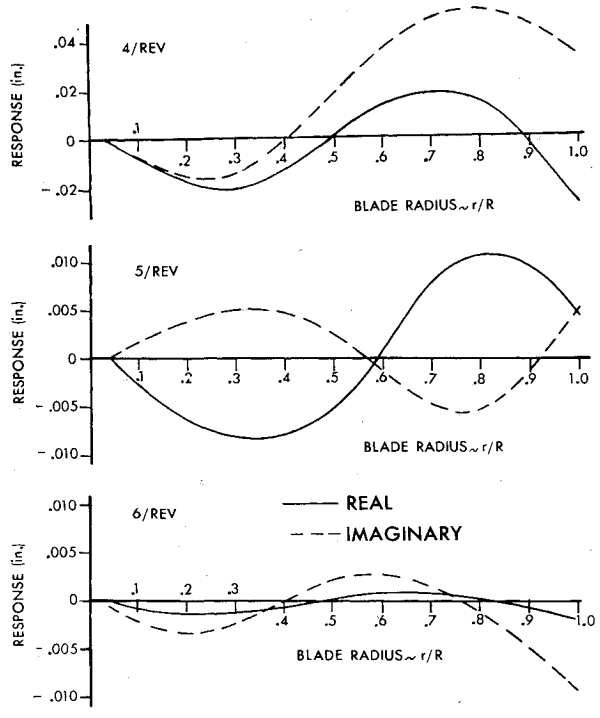

Fig. 10 Flatwise blade response; V = 150 knots, Ω = 222 rpm, gross wt = 13,600 lb.

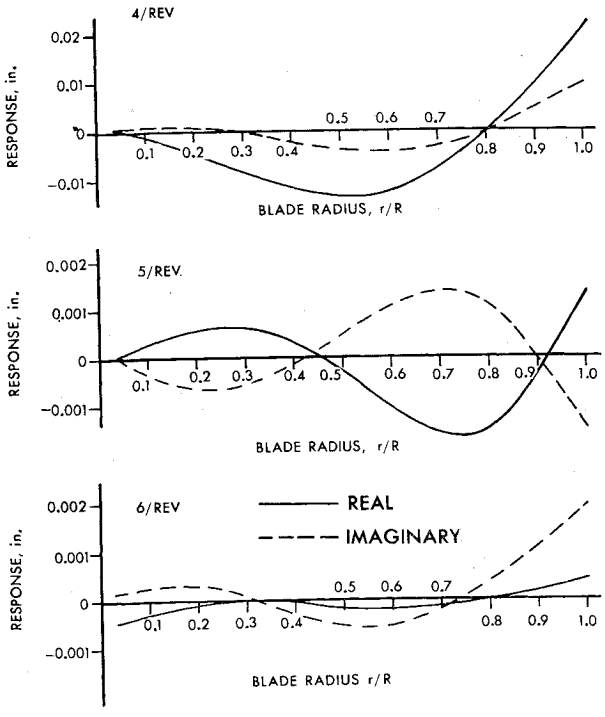

Fig. 11 Edgewise blade response; V = 150 knots, Ω = 222 rpm, gross wt = 13,600 lb.

Fuselage Dynamics

To calculate the coupled blade-fuselage forced response, it is first necessary to calculate the fuselage forced response at n/rev to the three unit fixed system forces and moments (S_x, S_y, S_z, M_{xx}, M_{yy}, M_{zz}). This yields the fuselage response or impedance matrix $[R]$. As has been seen, this is then used to obtain the coupled blade response and resulting blade root shears. Fixed system exciting forces are now obtained readily by using the $[\lambda]$ transformation matrix, Eq. (38). Final fuselage response is then calculated by multiplying the initial responses, obtained for unit loads, by the final fixed system forces and moments.

The method used for calculating the fuselage forced response is similar to that given in Ref. 5. Derivation of the method is presented in Appendix C. Response of the fuselage in relative coordinates is obtained by application of matrix equations (C15) and (C16). These are converted to absolute coordinates by matrix equation (C17).

Using this method, forced vibration response of a free-free beam is obtained by direct inverse solution of the fuselage dynamic matrix. Steps in the solution consist of the following:

1) Define the panel-point mass breakdown of the fuselage. From this form the mass matrix $[M]$.

2) Knowing the fuselage structural EI and GJ distribution, solve for influence coefficients for the previously designated panel-points. From this form the influence coefficient matrix $[K^{-1}]$.

3) Write fuselage absolute coordinates in terms of relative coordinates and obtain the transformation matrix $[\lambda]$. Carry along the ignorable or rigid-body coordinates as the last rows of this matrix.

4) Form the generalized mass matrix by carrying out the matrix multiplication $[\lambda'][M][\lambda]$. This yields the $[\overline{M}]$ matrix.

5) Form the force column matrix, knowing the coordinate locations and magnitudes of external exciting forces. Convert to generalized force by premultiplying by $[\lambda']$.

6) The problem now is that the generalized mass matrix is not compatible with the $[K^{-1}]$ matrix, being larger by rows and columns equal to the number of ignorable coordinates. These coordinates are separated by partitioning as shown in Appendix C. The solution can then be obtained by direct matrix substitution into matrix relations (C15–C17).

Separation of the rigid-body coordinates as given in Appendix C is in essence application of the free-free boundary conditions to the system. For a vertical vibration analysis, these would require that the sum of translational forces (external and inertia) be zero, and also that the sum of rotational moments be zero. Diagonal elements of the 2 × 2 matrix $[\delta]$ would be found to contain the total mass and mass moments of inertia of the system, respectively. The two off-diagonal elements would be equal and contain total static mass moments.

In summary, response of the fuselage to vibratory forces can be determined by the method described here, or by other standard vibration analysis techniques. A Myklestad-type solution, such as given for the rotor blades, might be used, as might a direct Newtonian or inertia-force method.

Part II: Discussion of Results

Comparisons with Flight Test Data

Figures 12 and 13 show a comparison at 110 knots between calculated airloads and those measured in flight on an H-34 helicopter blade. Constant inflow was taken in the analysis. The test helicopter was instrumented by Sikorsky Aircraft under U. S. Army TRECOM contract. Pressure pickups and strain gages were placed at various radial locations along the blade. Flight tests were conducted by NASA at Langley Field, and preliminary results of tests were released in Ref. 4. Measured data presented in Figs. 12 and 13 are for six of the seven pressure pickup locations. The comparison shows relatively good agreement between lower harmonics of measured and calculated airloads, particularly at blade outboard stations. But differences between the curves could contribute to substantial differences for the higher harmonics.

Results of blade stress correlation with constant inflow are illustrated in Figs. 14–16. Here, calculated and measured flatwise blade stresses are compared for the S-61 helicopter.

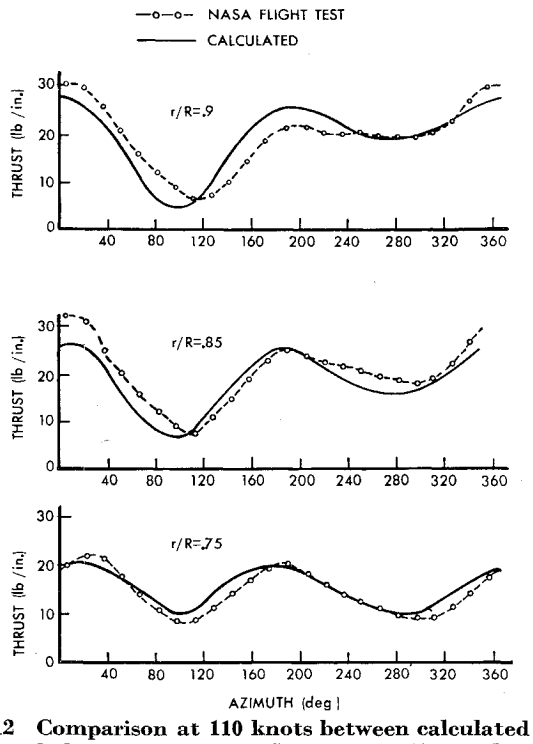

Fig. 12 Comparison at 110 knots between calculated airloads and those measured in flight on an H-34 helicopter blade.

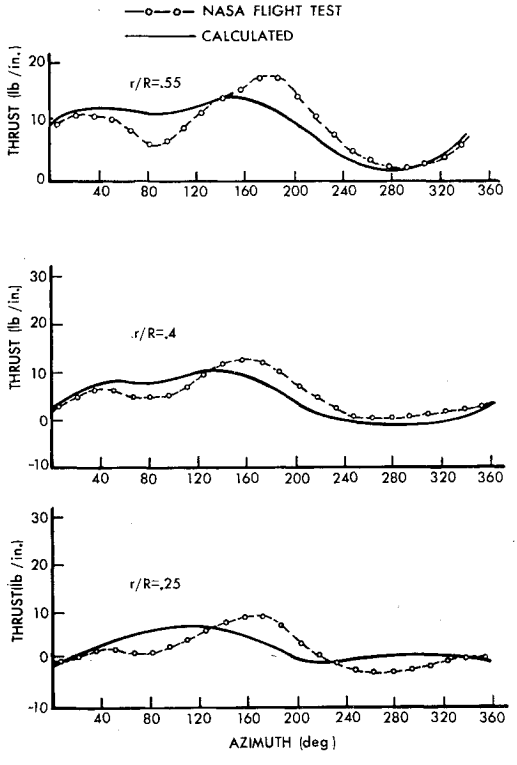

Fig. 13 Comparison at 110 knots between calculated airloads and those measured in flight on an H-34 helicopter blade.

For this case, as with the sample problem, analytical blade stresses were obtained by superposition of 11 harmonics of blade dynamic response. For rotor blade design, maximum vibratory stress is taken as one-half the peak-to-peak value per revolution at the critical blade station. Figure 14 gives a comparison between calculated and measured critical vibratory stress vs airspeed. Figures 15 and 16 present a comparison between calculations and test of the radial distribution of one-half peak-to-peak stress for the S-61 at 100 and 120 knots.

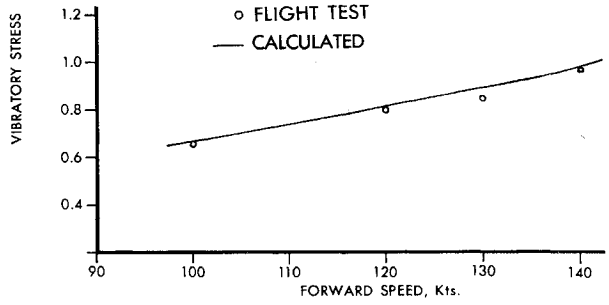

Fig. 14 Model no. S-61; 17,000 lb. = gross wt, Ω = 203 rpm.

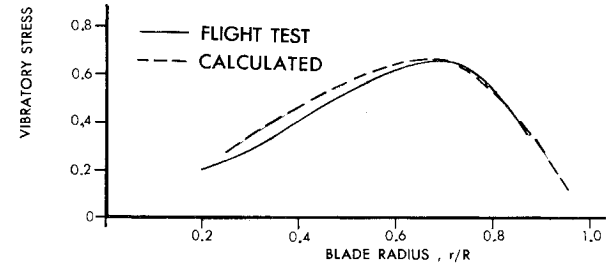

Fig. 15 Model no. S-61; 17,000 lb. = gross wt., Ω = 203 rpm, 100 knots.

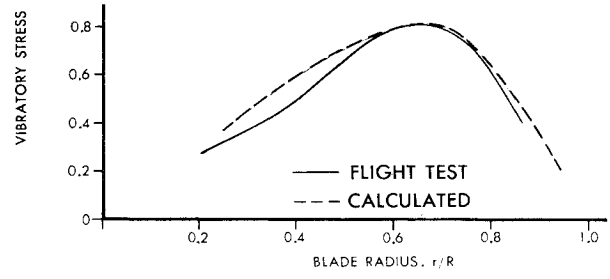

Fig. 16 Model no. S-61; 17,000 lb. = gross wt., Ω = 203 rpm, 120 knots.

Using constant inflow, the method of analysis described shows good agreement with measurements in predicting performance. This is illustrated by Fig. 17. Here, calculated and measured power are shown to compare favorably for the S-61 at 2-gross wt conditions. The computed values include power required for the tail rotor and accessory drives. Coefficients of drag were incremented by a $\Delta C_D = 0.002$ to account for additional roughness of the actual blade over a highly polished wind tunnel specimen. Note that good agreement is achieved even at low airspeeds, where effects of variable inflow have been shown to be large. This indicates that these airloads provide performance results consistent with standard performance calculations in use.

Sample Problem Results

Returning to the sample problem, Fig. 18 gives the change in location of the resultant thrust vector with increase in forward speed. As previously described, location of the thrust vector is estimated in initiating the aerodynamic solution then converged upon when the calculation is repeated. Location of the thrust vector can be more closely approximated on the first solution, if a curve such as shown in Fig. 18 is carried along as calculations proceed to higher airspeeds.

Figure 19 shows collective and cyclic pitch vs airspeed. Similar to the thrust vector plot, this may be carried along

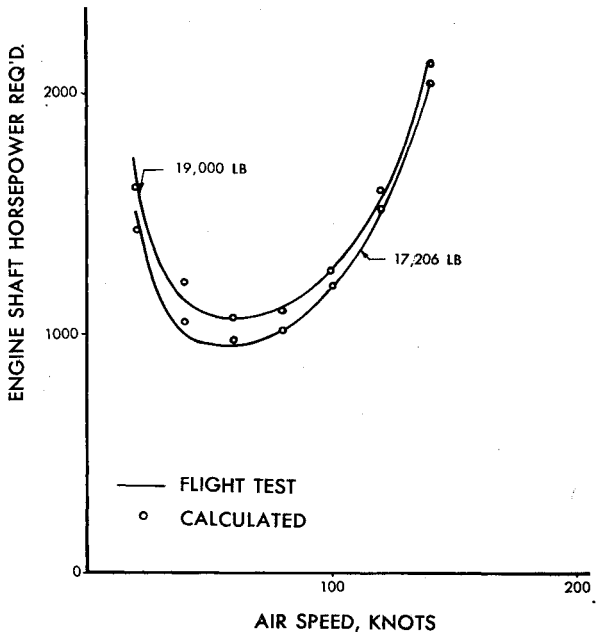

Fig. 17 S-61 helicopter performance comparison; gross weight as shown, Ω = 203 rpm.

for successive calculations. By this means, initial estimates of collective and cyclic pitch can be improved.

Figure 20 gives a plot of airload vs blade azimuth position for the 150-knot sample calculation. Results are shown at 90% blade radius. It will be noted that the character of this curve is similar to that shown by the flight test and calculated airloads of the H-34 at 110 knots.

Figure 21 presents the rotor trim Lissajous figures at three airspeeds: 80, 120, and 160 knots. The plots reveal that as airspeed increases, thrust moments on the advancing and retreating blades (ψ = 90° and ψ = 270°) diminish. Larger thrust moments are needed on the blade in the forward, ψ = 180°, and aft, ψ = 0°, positions to keep the rotor in equilibrium. These plots bear out the contention that the helicopter at high speeds flies on rotor blades in the ahead and behind positions.

Figure 22 presents a plot of total engine horsepower vs forward speed for the sample problem. For the plot, total engine horsepower was determined by 1) finding power required for the total drag torque of rotor; 2) adding to this the power required for a boundary-layer control system with a drag-equivalent of 1.6 ft², Ref. 14, p. 22; and 3) dividing this total by 0.9 to allow for tail rotor and accessory power.

Of interest in high-speed flight is rotor drag, shown plotted against forward speed in Fig. 23. Rotor drag is estimated in initiating the aerodynamic solution, then solved for after convergence of the cyclic pitch-thrust moment iteration. The curve of Fig. 23 is seen to rise very sharply at higher air-

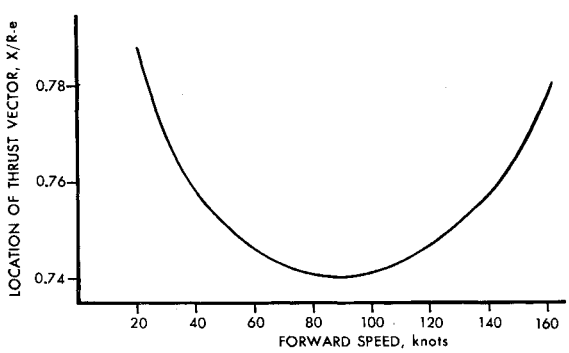

Fig. 18 Change in location of resultant thrust vector with increase in forward speed.

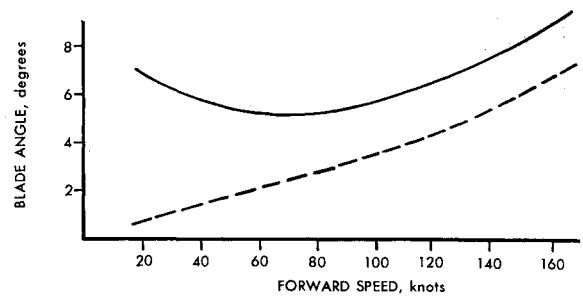

Fig. 19 Required collective pitch and required cyclic pitch vs airspeed.

speeds. Rotor drag is determined as follows.

Referring to Fig. 6, let the differential thrust and drag on a blade element at r be expressed as

$$dT = B_0(r) + \sum_{n=1}^{n=\infty} [A_n(r) \sin(n\psi) + B_n(r) \cos(n\psi)] \quad (42)$$

$$dD = b_0(r) + \sum_{n=1}^{n=\infty} [a_n(r) \sin(n\psi) + b_n(r) \cos(n\psi)] \quad (43)$$

Then

$$\text{Rotor drag} = \frac{b \cos\alpha_T}{2} \left[\sum_e^R a_1(r) - \sin\beta_0 \sum_e^R B_1(r) \right] \quad (44)$$

Figures 10 and 11 show the fourth (4/rev), fifth (5/rev), and sixth (6/rev) harmonics of calculated vibratory response for the blade of the sample problem. The real curves represent the $\sin(n\psi)$ component, and the imaginary represent the $\cos(n\psi)$ component. Both flatwise and edgewise deflection curves are shown. The flatwise forced response curves shown in Fig. 10 can be seen to be essentially second mode in character. This is explained by the fact that the natural frequency of the second flatwise bending mode is near the fifth harmonic (5/rev). The first flatwise bending frequency is between 2 and 3/rev, and the third is near 8/rev. Thus both are sufficiently removed from 4, 5, and 6/rev excitation. The edgewise blade responses of Fig. 11 are seen to be primarily first-to-second mode in character. The first edgewise bending natural frequency is between 3 and 4/rev. The strong influence of this mode can be seen in the 4/rev response. Shapes of the 5 and 6/rev edgewise responses are seen to be more second mode in character.

In studying the blade response curves it is interesting to note the effects of hub motion. This is indicated by the motion of the blade at the flapping hinges. For most cases plotted, it is barely detectable. But the 6/rev edgewise response shows substantial root motion. This indicates that coupling effects can be important when investigating higher mode response of rotor blades.

Plots representing the fuselage forced response for the sample problem are given in Figs. 24-27. Shown in Fig. 24 is the 5/rev vertical response of the fuselage. It will be

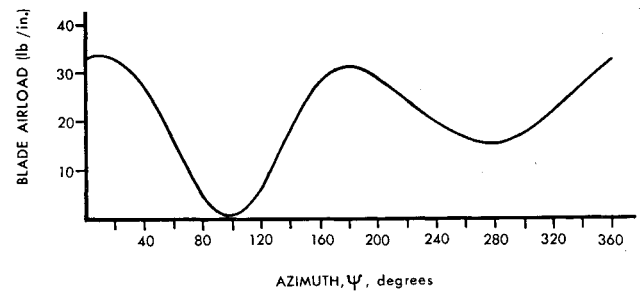

Fig. 20 Airload vs azimuth for hsh; v = 150 knots, −4° twist, r/R = 0.90.

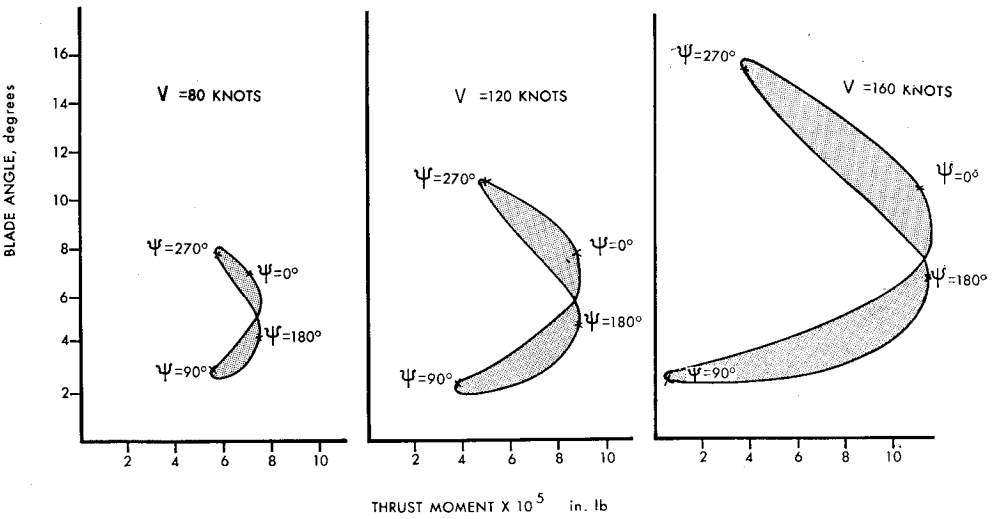

Fig. 21 Effect of forward speed on rotor trim.

noted, as with the blades, that the $\sin(n\psi)$ and $\cos(n\psi)$ fuselage motions are plotted separately. The fuselage of the sample problem has a first vertical bending mode at 500 cpm and a second vertical bending mode at 1241 cpm. The 5/rev exciting frequency is 1110 cpm. The resulting fuselage forced response can be seen to be first-to-second mode in character.

Figures 26 and 27 show corresponding 5/rev lateral-torsion response of the hsh fuselage. Lateral and torsional components of the coupled response have been plotted separately. For the fuselage considered, the first lateral mode response of the coupled lateral-torsion system occurs at 342 cpm, the second at 1268. For the torsional component, corresponding frequencies are at 817 cpm and 1942 cpm, respectively. Thus, for both components the frequency of excitation lies between the first and second modes.

Given in Fig. 25 is a plot of vertical cockpit vibration levels vs forward speed. Values given will be noted to be quite low, 0.035 g's at 150 knots. As will be discussed later, these low calculated vibration levels are attributed to constant inflow. Studies show that variable inflow must be taken into account to accurately predict fourth, fifth, and sixth harmonics of rotor blade airloads.

Figures 28–30 are the results of blade stress calculations for the sample problem. Figure 28 shows flatwise bending stress vs blade azimuth position at the blade station of maximum vibratory stress for the 150-knot condition. Indicated on the plot is the manner in which the one-half peak-to-peak stress is determined. Figure 29 gives the radial distribution of one-half peak-to-peak stress at three airspeeds; 120, 150, and 170 knots. It can be seen from the plots that there is an outward shift of the point of maximum stress as airspeed increases. Increase in maximum flatwise vibratory stress with increase in airspeed is presented in Fig. 30.

General Discussion

Primary emphasis in this paper has been on development of method. A method of analysis has been described, which can be used to explore effects of flight, rotor, blade, and fuselage parameters on resulting blade motions, blade stresses, fuselage vibrations, and performance of articulated and rigid rotor systems.

In deriving the basic equations, certain key points were kept in mind. The equations in general, and in particular for the blade, are set up to be as flexible as possible so that the analysis is suitable for studies of a wide range of helicopters and VTOL-type aircraft. There are provisions for handling rotor and propeller blades of all types: rigid, teetering, and articulated. Small angle assumptions were avoided in many portions of the analysis to accommodate a wide range of flight conditions and configurations such as a tilt-wing aircraft.

Other features are included in the analysis. In the calculation of aerodynamic loads there is provision for variable inflow. Blade stall and compressibility are included by taking into account reverse flow and Mach number. Two-dimensional airfoil data are incorporated for angles-of-attack up to 360°, since a wide range of angles-of-attack of blade element are encountered by the rotor at high advance ratios. Addition of extra blade stations or degrees of freedom does not increase the number of blade simultaneous equations to be solved. The elastic analysis requires writing the equations for forces and moments on an element. The computer performs the integration. Flatwise-edgewise blade deflections with coupling due to twist are included. Blade loads and motions are coupled to the rotor head. For the combined blade and fuselage forced response, a closed form solution is used. Complex notation is used to provide proper

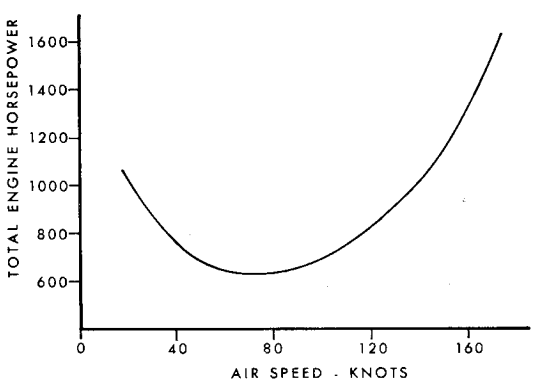

Fig. 22 Forward flight performance, sea level.

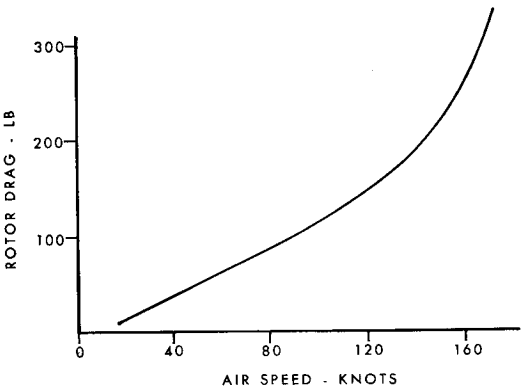

Fig. 23 Effect of air speed on rotor drag.

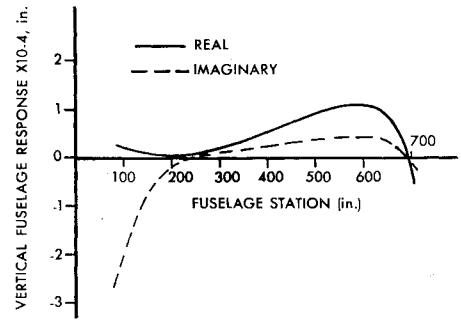

Fig. 24 Vertical fuselage response.

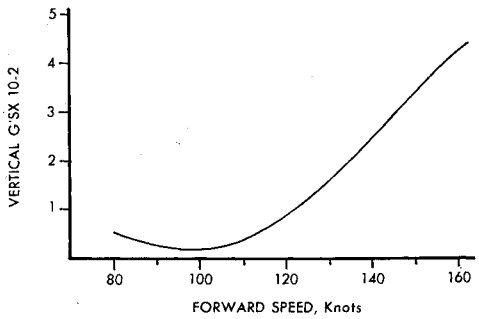

Fig. 25 Cockpit vibration levels vs forward speed.

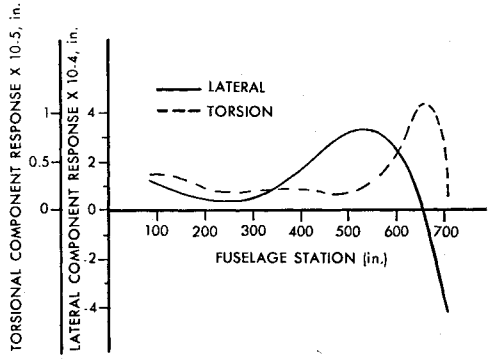

Fig. 26 Real or $\sin(n\psi)$ coupled lateral-torsion response.

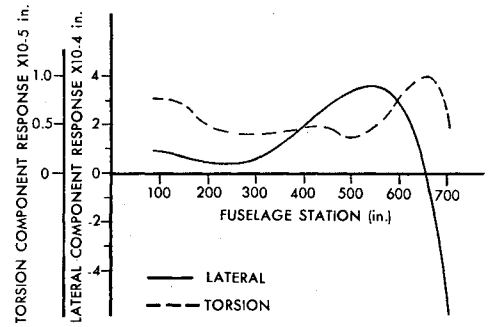

Fig. 27 Imaginary or $\cos(n\psi)$ coupled lateral-torsion response.

phasing of element responses for the blades and fuselage, simplifying the introduction of aerodynamic and lag damping in the blade equations. Similarly, structural damping is provided in the fuselage dynamic response.

The blade analysis, which has been described, can also be used to calculate blade flatwise and edgewise natural frequencies by the method of Ref. 7. To find a natural frequency of the rotor blade, a frequency ω is assumed, and shears, moments, slopes and deflections are calculated, element by element from the tip of the blade to the root. Application of root boundary conditions yields a determinant

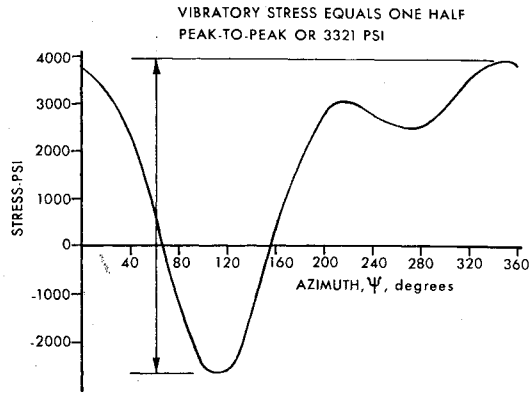

Fig. 28 Stress vs azimuth for the critical blade station, $x/r = 0.62$ at 150 knots.

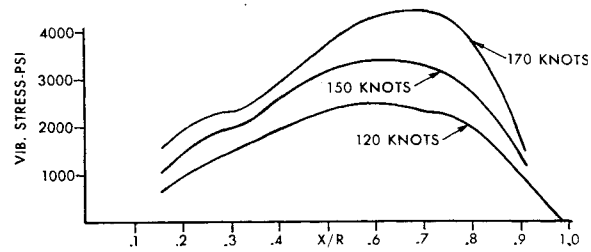

Fig. 29 Radial plot of vibratory stress at three airspeeds.

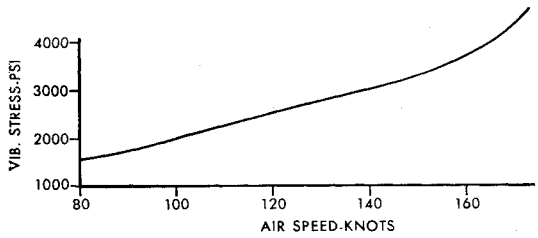

Fig. 30 Maximum vibratory stress vs airspeed.

at the root. The condition to satisfy the equations is that the determinant must go to zero. When this occurs one has a natural frequency. The method given in Ref. 11 can be used for obtaining a good first estimate of frequency.

The coupled blade-fuselage vibration analysis may be applied to other types of rotor systems. Consider the case of infinite rotor head impedance for several types of rotor systems. Here, boundary conditions become as follows:

Teetering Rotor with n-Blades

$$\theta_0^F = 0 \qquad Z_0 = 0 \qquad \theta_0^E = 0 \qquad X_0 = 0 \quad (45)$$

for $0, n, 2n, 3n \ldots$, etc., harmonics.

$$M_0^F = 0 \qquad Z_0 = 0 \qquad \theta_0^E = 0 \qquad X_0 = 0 \quad (46)$$

for all other harmonics.

Rigid Rotor

$$\theta_0^F = 0 \qquad Z_0 = 0 \qquad \theta_0^E = 0 \qquad X_0 = 0 \quad (47)$$

Articulated Blade with Centering Spring

$$M_0^F = 0 \qquad Z_0 = 0$$
$$M_0^E - K_\theta \theta_0^E = 0 \qquad X_0 = 0 \quad (48)$$

Freely Flapping Blade, Chordwise Restraint

$$M_0^F = 0 \qquad Z_0 = 0 \qquad \theta_0^E = 0 \qquad X_0 = 0 \quad (49)$$

Conventional Articulated Blade with Vertical Spring and Damper at Hinge

$$M_0^F = 0 \qquad S_0^F - K_v Z_0 - jC_v \omega Z_0 = 0$$
$$M_0^E - jC_\theta \omega \theta_0^E = 0 \qquad X_0 = 0 \quad (50)$$

For each rotor system, coupling of blades to the fuselage would be taken into account by 1) relating forces and moments at the root of the blade in rotating coordinates to the three fixed system shears and three fixed system moments acting at the center of the rotor head; 2) relating displacements and rotations at the root of the blade in rotating coordinates to fixed system displacements and rotations at the center of the rotor head; and 3) following the procedure outlined in this paper for calculating the coupled blade-fuselage response.

A brief discussion of accuracy follows. The coupled blade-fuselage response requires inverting a 12 × 12 complex blade matrix. It has been pointed out by Horvay[8] and others that considerable accuracy is necessary in solution of a rotor blade's forced response. Horvay recommends 10 decimal digits. The method used here is similar, being essentially a step-by-step integration of the blade dynamic equations, from tip to root. Accuracy problems were compounded in this case by coupling three blade dynamic responses together. Here, conventional matrix inversion techniques were found to be inadequate, even using double precision (17 decimal digits). This was attributed to the large products obtained, and small differences of large numbers. However, Crout's method[12, 16] was found to be satisfactory, even in single precision (8 + decimal digits). This method does not depend on carrying out long repeated multiplications. Instead, it is based on first normalizing, then subtracting successive equations.

No discussion on helicopter dynamics is complete without some comments on the problem of variable induced velocity. For the high-speed helicopter, the two major problems are developing sufficient power to attain the desired speed and limiting blade stresses to a low enough value for structural reliability. These two problems are adequately

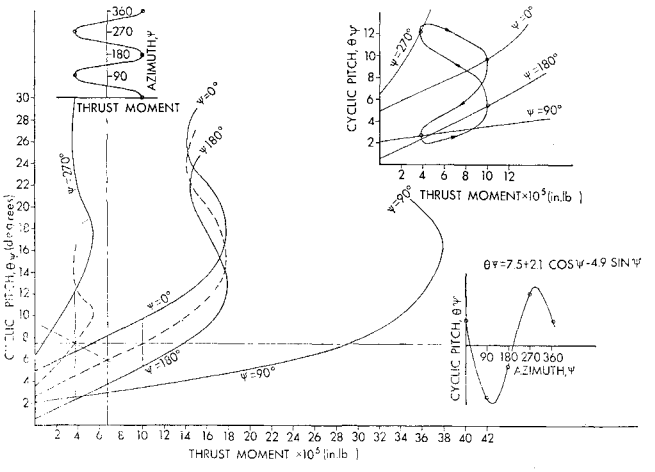

Fig. 31 Four point graphical solution for rotor trim.

defined by the assumptions made in this paper of constant induced velocity. However, in order to investigate fuselage response and cabin vibratory levels, the higher harmonics of blade loadings must be more accurately defined. Better description of these higher harmonics depends on variable induced velocity.

The aeroelastic flow chart of Fig. 3 shows that either variable induced velocity or constant induced velocity may be used to generate the aerodynamic loads. Sufficient calculations have been run with various types of induced velocity assumptions to show that blade stresses and power available depend largely on the steady, first- and second-harmonic components. Above 100 knots, these can be defined with sufficient accuracy by a constant induced velocity program. These programs also show that much higher responses are obtained in the fuselage using variable induced velocities, and that these increases are necessary to correlate with actual flight conditions. Results of the computation for fuselage response with constant induced velocity are shown in Fig. 25 and indicate very low levels. A helicopter would normally experience about ±0.5 g at 160 knots. These levels can be obtained by reasonable but not completely justifiable assumptions in the variable induced velocity. Responses in the transition range below 70 knots were not plotted because in this region it is fairly obvious that variable induced velocity definition must be used.

The analysis presented herein is dependent on the IBM 7090 computer for providing the designer with an accurate and useable tool. Results of variable inflow analysis such as given in Refs. 1–3 and 10 are encouraging. These indicate the problem can be solved by extensive machine calculations. But simpler and more accurate procedures are required in variable inflow analysis before the designer will have a practical tool for the complete problem, even with the aid of high-speed computers.

Conclusions

A method of analysis has been described, which makes it possible to consider helicopter aerodynamics, blade dynamics, and fuselage dynamics simultaneously. The method has been carried through for a typical high-speed helicopter.

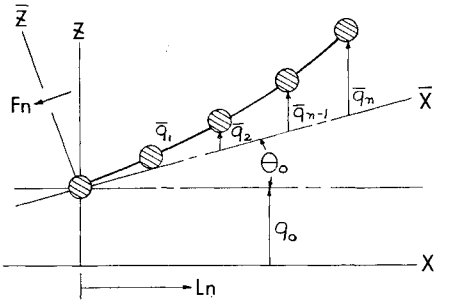

Fig. 32 Fuselage forced vibration analysis.

In addition, results have been compared with flight test data from an H-34 and S-61 helicopter. Conclusions from these studies are as follows:

I) Using constant induced velocity, 1) the analysis satisfactorily predicts lower harmonics of airloads at speeds above 100 knots; 2) good agreement was achieved between measured and calculated one-half peak-to-peak flatwise vibratory blade stresses at speeds above 100 knots; 3) the analysis correlates well with measured helicopter performance, even at speeds below 100 knots; and 4) predicted fuselage inflight vibration levels are much lower than flight-measured values.

II) In view of the lack of larger higher harmonic responses of blades and fuselage, it is apparent that the most probable area of improvement is a better definition of induced velocity distribution in order to 1) accurately predict higher frequency airloads and blade stresses at all airspeeds; 2) correlate one-half peak-to-peak blade stresses below 100 knots; and 3) analytically determine inflight fuselage vibration levels at all airspeeds.

III) Treatment of the entire helicopter aeroelastic problem, as described, is made possible only by use of high-speed digital computers. The many calculations include 1) an aerodynamic iteration at close azimuth intervals; 2) step-by-step integration of 24 blade stations by 8 simultaneous equations; 3) inverting a 12 × 12 complex matrix; and 4) solving the response of a multi-degree-of-freedom fuselage dynamic system. The addition of variable inflow, by extending the numerical work required, will further enforce the need for high-speed computers.

Appendix A: Graphical Method for Solution of Rotor Trim

Solution of rotor trim by the graphical method is shown in Fig. 31. The sample presented is a four-point approximate solution for 90° blade azimuth intervals. The method can readily be extended to an eight-point determination. Results are shown for the sample hsh helicopter at 150 knots.

First step in setting up the problem is to construct from Eq. (6) lines of θ_ψ vs thrust moment at 0, 90, 180, and 270°. Next, assuming the thrust to act at 0.7 radius, a vertical line is erected, which represents the mean thrust moment required from the rotor. For the example as shown in Fig. 31, this value is at 6.8×10^5 in.-lb.

Now a median line is drawn between the $\psi = 0°$ and $\psi = 180°$ lines. A similar median line is constructed representing the average of the $\psi = 90°$ and $\psi = 270°$ lines. Following this, a mirror image line is reflected back from the intersection of the 0–180 median and the mean thrust moment vertical. The intersection of this reflected line with the 90–270 median represents the collective pitch required for flight. A vertical line erected through this point immediately gives the values of cyclic pitch required at 90 and 270°. Similarly, a vertical erected through the intersection of the 0–180 median and the collective line yields cyclic pitch required at 0 and 180°. With this, constants necessary to define the cyclic pitch are readily obtained as shown in Fig. 31 and given as

$$\theta_\psi = \theta_0 + \theta_{1s} \sin\psi + \theta_{1c} \cos\psi \tag{A1}$$

Shown in the upper right-hand corner of Fig. 31 is the Lissajou figure, which results from the graphical solution. Here it will be noted, the 90 and 270° points, as well as the 0 and 180° points, fall vertically in line. As only four points have been used in the approximate graphical solution, there can be no thrust moment components above the second harmonic.

Appendix B: Rotor Blade Twist Coupling

Slope and deflection relationships for the blade and resultant twist coupling terms are derived as follows. Let v, u, and g§ be slope due to moment, slope due to load, and deflection due to load, respectively, of the blade about its flatwise principal axis. Also, let V, U, and G be corresponding values about the blade's chordwise principal axis. Allowing for one discontinuity η in a station length $l_{n,n+1}$, one obtains

$$v_{n,n+1} = \left[\frac{\eta_{n,n+1}}{(EIy)_{n+1}} + \frac{l_{n,n+1} - \eta_{n,n+1}}{(EIy)_n}\right] \tag{B1}$$

$$u_{n,n+1} = \frac{1}{2}\left[\frac{\eta^2_{n,n+1}}{(EIy)_{n+1}} + \frac{l^2_{n,n+1} - \eta^2_{n,n+1}}{(EI_y)_n}\right] \tag{B2}$$

$$g_{n,n+1} = \frac{1}{3}\left[\frac{\eta^3_{n,n+1}}{(EIy)_{n+1}} + \frac{l^3_{n,n+1} - \eta^3_{n,n+1}}{(EIy)_n}\right] \tag{B3}$$

The expressions for V, U, and G are the same, except that EIy is replaced by EIx. Now, take the blade element feathered at an angle, β, to the reference plane at right angles to the axis of rotation (Fig. 4). Here, β would include twist β_T and blade feathering θ. Then, the slope and deflection relationships, as given in Eqs. (B4–B12), are

$$V_{zz} = V_{n,n+1} \sin^2\beta + v_{n,n+1} \cos^2\beta \tag{B4}$$

$$V_{zx} = V_{xz} = (V_{n,n+1} - v_{n,n+1}) \sin\beta \cos\beta \tag{B5}$$

$$u_{zz} = U_{n,n+1} \sin^2\beta + u_{n,n+1} \cos^2\beta \tag{B6}$$

$$u_{zx} = U_{xz} = (U_{n,n+1} - u_{n,n+1}) \sin\beta \cos\beta \tag{B7}$$

$$g_{zz} = G_{n,n+1} \sin^2\beta + g_{n,n+1} \cos^2\beta \tag{B8}$$

$$g_{zx} = G_{xz} = (G_{n,n+1} - g_{n,n+1}) \sin\beta \cos\beta \tag{B9}$$

$$V_{xx} = V_{n,n+1} \cos^2\beta + v_{n,n+1} \sin^2\beta \tag{B10}$$

$$U_{xx} = U_{n,n+1} \cos^2\beta + u_{n,n+1} \sin^2\beta \tag{B11}$$

$$G_{xx} = G_{n,n+1} \cos^2\beta + g_{n,n+1} \sin^2\beta \tag{B12}$$

§ See Ref. 8, Eqs. (9a–c).

Appendix C: Forced Vibration Analysis with Damping (See Fig. 32)

Fuselage Forced Vibration Analysis

q_n = absolute generalized coordinate
$\bar{q}_n$ = relative generalized coordinate
m_n = lumped masses assigned to stations, n
k_n = spring constants assigned to stations, n
F_n = external vibratory forces or moments at particular stations, n

Kinetic Energy

$$2T = [\dot{q}][M]\{\dot{q}\} \tag{C1}$$

Potential Energy

$$2V = [\bar{q}][K]\{\bar{q}\} \tag{C2}$$

Dissipation Function

$$2D = [\dot{\bar{q}}]jg[K]\{\bar{q}\} \tag{C3}$$

Work

$$W = [q]\{F\} \tag{C4}$$

The coordinates must be transformed to a common energy plane:

$$\begin{aligned}
q_1 &= q_0 + \theta_0 l_1 + \bar{q}_1 \\
q_2 &= q_0 + \theta_0 l_2 + \bar{q}_2 \\
q_3 &= q_0 + \theta_0 l_3 + \bar{q}_3 \\
&\cdots \\
q_{n-1} &= q_0 + \theta_0 l_{n-1} + \bar{q}_{n-1} \\
q_n &= q_0 + \theta_0 l_n + \bar{q}_n
\end{aligned}$$

Introduce dummy, or ignorable coordinates, q_0, θ_0. In matrix form

$$\begin{bmatrix} q_1 \\ q_2 \\ q_3 \\ \cdot \\ \cdot \\ \cdot \\ q_{n-1} \\ q_n \\ q_0 \\ \theta_0 \end{bmatrix} = \begin{bmatrix} 1 & 0 & 0 & \cdots & 0 & 0 & 1 & l_1 \\ 0 & 1 & 0 & \cdots & 0 & 0 & 1 & l_2 \\ 0 & 0 & 1 & \cdots & 0 & 0 & 1 & l_3 \\ \cdots & & & & & & & \cdots \\ 0 & 0 & 0 & & 1 & 0 & 1 & l_{n-1} \\ 0 & 0 & 0 & & 0 & 1 & 1 & l_n \\ 0 & 0 & 0 & & 0 & 0 & 1 & 0 \\ 0 & 0 & 0 & & 0 & 0 & 0 & 1 \end{bmatrix} \begin{bmatrix} \bar{q}_1 \\ \bar{q}_2 \\ \bar{q}_3 \\ \cdot \\ \cdot \\ \cdot \\ \bar{q}_{n-1} \\ \bar{q}_n \\ \bar{q}_0 \\ \bar{\theta}_0 \end{bmatrix}$$

or

$$\{q\} = \lambda\{\bar{q}\} \tag{C5}$$

and

$$\{\dot{q}\} = \lambda\{\dot{\bar{q}}\} \tag{C6}$$

also

$$[q] = [\bar{q}]\lambda' \tag{C7}$$

from which,

$$2T = [\dot{\bar{q}}]\lambda'[M]\lambda\{\dot{\bar{q}}\} \tag{C8}$$

Let $\lambda'[M]\lambda = [\bar{M}]$, then

$$2T = [\dot{\bar{q}}][\bar{M}]\{\dot{\bar{q}}\} \tag{C9}$$

Work

$$W = [q]\{F\} = [\bar{q}]\lambda'\{F\} \tag{C10}$$

Generalized Force

$$\{\Phi\} = \partial W/\partial \bar{q} = \lambda'\{F\} \tag{C11}$$

Applying LaGrange's equation,

$$\frac{d}{dt}\left(\frac{\partial T}{\partial \dot{\bar{q}}}\right) - \frac{\partial T}{\partial \bar{q}} + \frac{\partial V}{\partial \bar{q}} + \frac{\partial D}{\partial \bar{q}} = \frac{\partial W}{\partial \bar{q}}$$

$$[\bar{M}]\{\ddot{\bar{q}}\} + [K]\{\bar{q}\} + jg[K]\{\bar{q}\} = \{\Phi\}$$

Assume,

$$\{\bar{q}\} = \{\bar{Q}\}e^{j\omega t}$$

then

$$-\omega^2[\bar{M}]\{\bar{Q}\} + [K]\{\bar{Q}\} + jg[K]\{\bar{Q}\} = \{\Phi\} \tag{C12}$$

Partitioning the matrices so as to separate those portions that contain ignorable coordinates,

$$-\omega^2\left[\begin{array}{c|c}\alpha & \beta \\ \hline \beta' & \delta\end{array}\right]\left[\begin{array}{c}\bar{Q}_1 \\ \hline \bar{Q}_2\end{array}\right] + \left[\begin{array}{c|c}K & 0 \\ \hline 0 & 0\end{array}\right]\left[\begin{array}{c}\bar{Q}_1 \\ \hline \bar{Q}_2\end{array}\right] + jg\left[\begin{array}{c|c}K & 0 \\ \hline 0 & 0\end{array}\right]\left[\begin{array}{c}\bar{Q}_1 \\ \hline \bar{Q}_2\end{array}\right] = \left[\begin{array}{c}\Phi_1 \\ \hline \Phi_2\end{array}\right]$$

Solving the simultaneous equations for $\bar{Q}_1$,

$$-\omega^2(\alpha - \beta\delta^{-1}\beta')\{\bar{Q}_1\} + (I + jg)[K]\{\bar{Q}_1\} = \Phi_1 - \beta\delta^{-1}\Phi_2 \tag{C13}$$

where I is a unit matrix.

$$\underbrace{\left[\frac{I}{\omega^2} - [K^{-1}](\alpha - \beta\delta^{-1}\beta') + \frac{jg}{\omega^2}\right]}_{[E]}\{\bar{Q}_1\} = \frac{[K^{-1}](\Phi_1 - \beta\delta^{-1}\Phi_2)}{\omega^2} \tag{C14}$$

$$[E]\{\bar{Q}_1\} = \frac{[K^{-1}](\Phi_1 - \beta\delta^{-1}\Phi_2)}{\omega^2}$$

from which

$$\{\bar{Q}_1\} = \frac{[E^{-1}][K^{-1}](\Phi_1 - \beta\delta^{-1}\Phi_2)}{\omega^2} \tag{C15}$$

where $[K^{-1}]$ is the influence coefficient matrix

$$\{\bar{Q}_2\} = (-\delta^{-1}\Phi_2/\omega^2) - \delta^{-1}\beta'\{\bar{Q}_1\} \tag{C16}$$

and

$$\{Q\} = \lambda\{\bar{Q}\} \tag{C17}$$

determines the absolute displacements of each panel point.

References

[1] Miller, R. H., "Rotor blade harmonic airloading," IAS Paper 62–82 (January 1962).

[2] Willmer, M. A. P., "The loading of helicopter rotor blades in forward flight," Royal Aircraft Establishment Rept. Naval 2-n-76935 no. 8 (April 1959).

[3] Piziali, R. and DuWaldt, F., "Computation of rotary wing harmonic airloads and comparison with experimental results," *Proceedings of the American Helicopter Society, Eighteenth Annual National Forum* (American Helicopter Society, New York, 1962).

[4] "Information and preliminary data on helicopter rotor blade dynamic airloads and moments as measured in flight," U. S. Army Transportation Res. Command, NASA (May 24, 1961), p. 9.

[5] Mack, C. E., "Tensor analysis of aircraft structural vibration," Sherman M. Fairchild Fund, IAS Paper 104 (October 1946).

[6] Wheatley, J. B., "An aerodynamic analysis of the autogiro rotor with a comparison between calculated and experimental results," NACA Rept. 487 (1934).

[7] Myklestad, N. O., "A new method of calculating natural modes of uncoupled bending vibrations of airplane wings and other types of beams," J. Aeronaut. Sci. II, 153–162 (1944).

[8] Horvay, G., "Stress analysis of rotor blades," J. Aeronaut. Sci. **14**, 315–336 (1947).

[9] Myklestad, N. O., *Vibration Analysis* (McGraw-Hill Book Co. Inc., New York, 1956), Chapt. 8, pp. 244–247.

[10] Tararine, J. and Delest, M., "Experimental and theoretical study of local induced velocity over a rotor disc for analytical evaluation of the primary loads acting on helicopter rotor blades," Giravions Dorand Co. Rept. DE 2012 (1960).

[11] Yntema, R., "Simplified procedures and charts for the rapid estimation of bending frequencies of rotating beams," NACA TN 3459 (1955).

[12] Scanlon, R. H. and Rosenbaum, R., *Introduction to the Study of Aircraft Vibration and Flutter* (MacMillan Co., New York, 1951).

[13] Critzos, C., Heyson, H., and Boswinkle, R., Jr., "Aerodynamic characteristics of NACA 0012 airfoil section at angles of attack from 0° to 180°," NACA TN 3361 (1955).

[14] Fradenburgh, E. A., "High performance single rotor helicopter study," Transportation Res. Command Rept. TREC TR 61-44 (April 1961).

[15] Fradenburgh, E. A. and Rabbott, J. P., Jr., "High-speed helicopter research," paper presented to American Helicopter Society, 18th Annual National Forum (May 1962).

[16] Crout, P. L., "A short method for evaluating determinants and solving systems of linear equations with real or complex coefficients," Trans. Am. Inst. Electrical Engrs. **60**, 1235–1241 (1941).